6. EVALUATIONS OF PLASTIC FATIGUE PROPERTIES OF HEAT-RESISTANT ALLOYS

(1516)

J. B. Conway*

The objective of this program is to determine the parameters affecting low-cycle fatigue life of metals and alloys at elevated temperatures and to generate low-cycle fatigue data for use in the design of structural components of high-performance nuclear reactor systems.

Materials currently being studied in this program are the AISI 304, 348, and 316 stainless steels. Test parameters under investigation are temperature, strain amplitude, strain rate, and length of hold times at peak strain in each cycle.

6.1 MATERIAL SPECIFICATIONS

AISI 304 STAINLESS STEEL ROD STOCK

AISI grade – heat 55697 from PNL – billets 49 cm^2 cross-sectional area, rolled at 1180°C to rods 16 mm in diameter – rod coiled, annealed 60 minutes at 1066°C, and water quenched – sections cut from coil, straightened, stress-relieved 30 minutes at 1010°C, and water quenched.

AISI 348 STAINLESS STEEL ROD STOCK

AISI grade – heat 55700 from PNL – rolling and heat treatment sequence same as for Type 304 stainless steel.

AISI 316 STAINLESS STEEL ROD STOCK

AISI grade – heat 65808 from PNL – ladle chemistry by weight percent:

C	Mn	Si	Cr	Ni	Mo	Co	Sn	Cu	S	P	N_2
0.086	1.73	0.52	18.16	13.60	2.47	0.74	0.040	0.078	0.006	0.010	0.050

NMPO PROCESSING – AISI 304 AND 348 STAINLESS STEEL

Ground specimens to hourglass configuration – diametral gage section 0.635 cm – surface of gage section longitudinally polished – annealed 30 minutes at 1092°C in argon, cooling rate approximately 100°C per minute – average VHN 139 for 304 SS and 155 for 348 SS – grain size ASTM 3-5.

NMPO PROCESSING – AISI 316 STAINLESS STEEL

Sample blanks annealed 30 minutes at 1070°C in air and water quenched – ground samples to hourglass configuration – diametral gage section 0.635 cm – surface of gage section longitudinally polished – stress relieved 60 minutes at 760°C in argon, cooling rate approximately 100°C per minute – average VHN 171 – grain size ASTM 3-5.

*Project leader and principal investigator.

6.2 FATIGUE-TESTING EQUIPMENT

During the past year equipment and test technique modifications were made to improve the precision and accuracy of low-cycle fatigue data being generated. A more precise method was devised for calibrating the extensometer employed to measure diametral strain; Figure 6.1 shows a photograph of the new calibration fixture. This fixture has permitted the extensometer to be calibrated in a manner that closely simulates the mode of operation during an actual test.

Another improvement consisted of fabricating Plexiglas enclosures for two uniaxial fatigue systems. One enclosure shown in Figure 6.2 permits operation in air while isolating the testing or sample zone from the immediate laboratory environment. In this way the effects of the unavoidable air currents present in the laboratory are eliminated and the test specimen temperature is more accurately controlled. This modification also permits tests to operate in inert environments if such testing becomes desirable.

Another modification which promises to improve testing accuracy involves the repositioning of the load-measuring device in the load train. This change was needed to eliminate the extraneous load resulting from frictional forces in the die-set assembly; this is presently summed along with the force on the test specimen. A sketch of this new modification is presented in Figure 6.3. The new die-set fixture is being assembled and will soon be incorporated into the current test program.

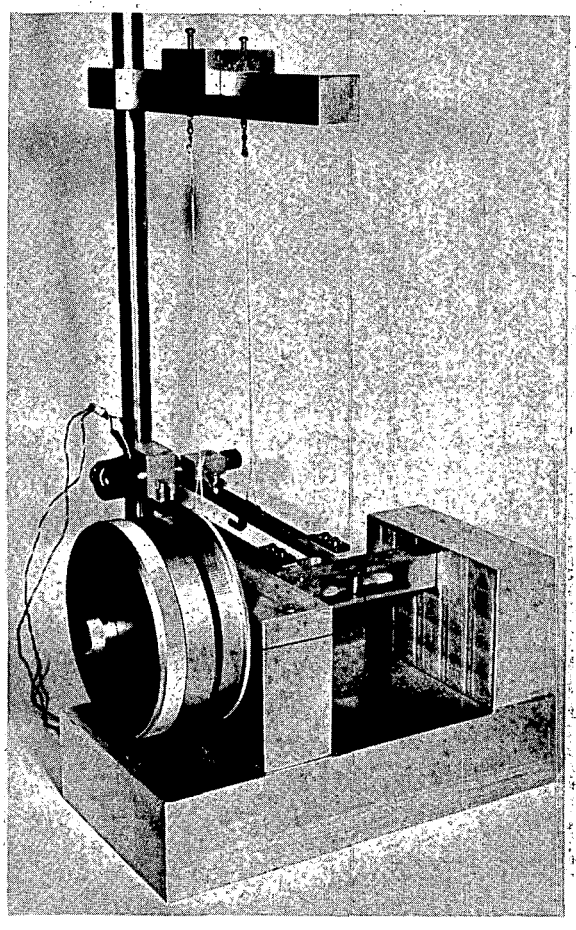

Fig. 6.1 – Calibration fixture for diametral strain extensometer (Neg. P68-2-2D)

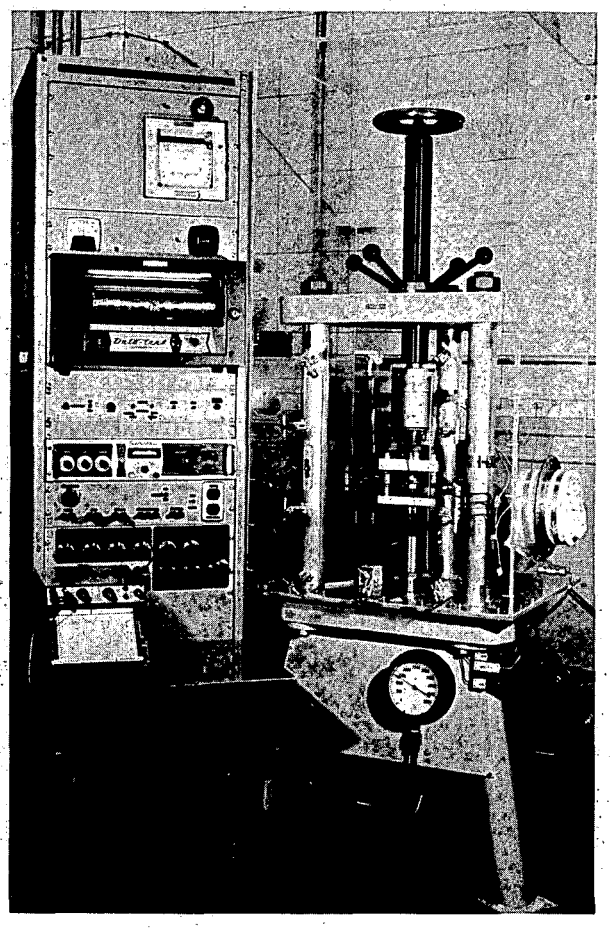

Fig. 6.2 – Typical uniaxial fatigue-testing system with Plexiglas enclosure (Neg. P68-2-2C)

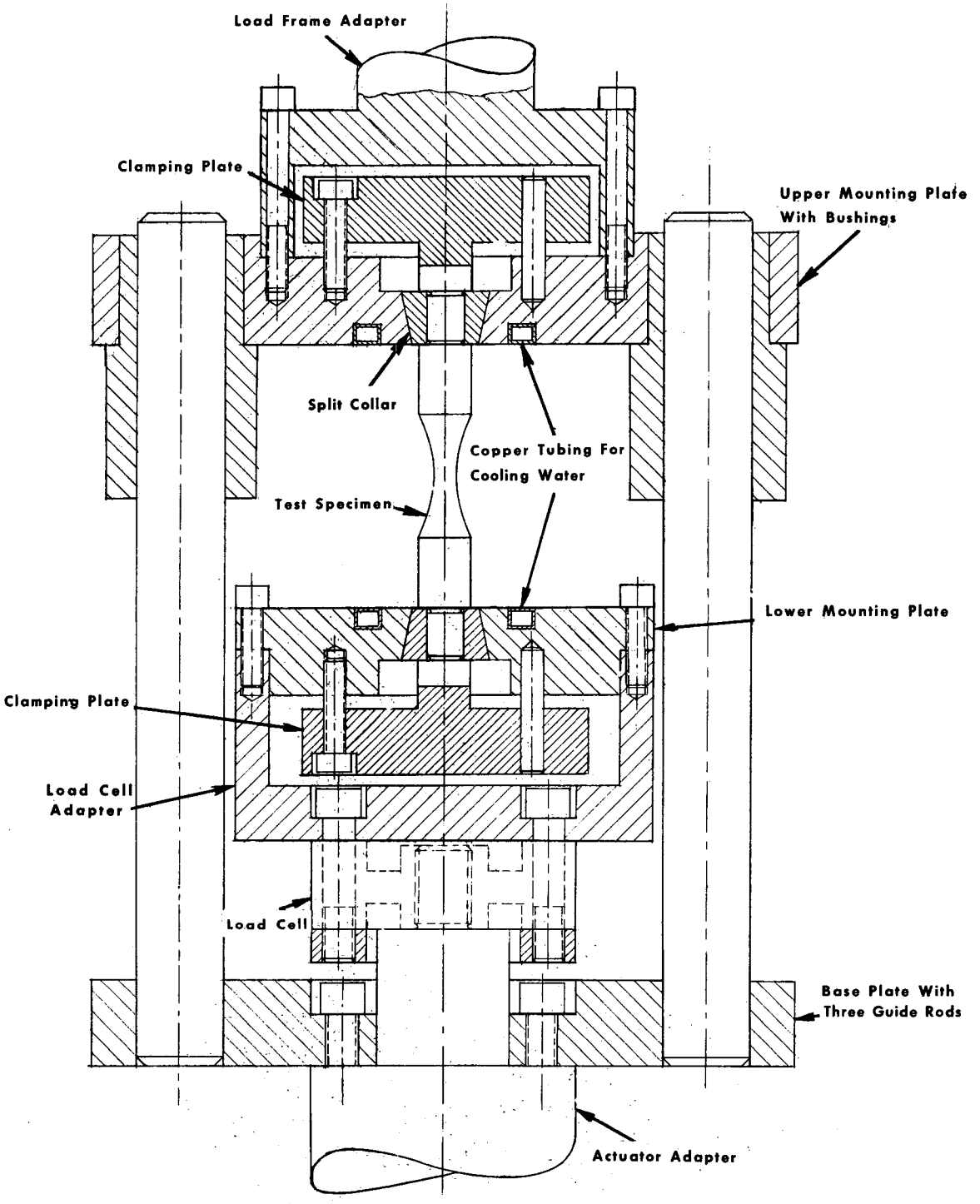

Fig. 6.3 – Sketch of test specimen and loading fixture

In another important equipment modification, a strain computer shown in Figure 6.4 was developed and installed on each fatigue-testing machine. This small analog computer continually determines relative amounts of elastic and plastic strain in the specimen and produces a signal which represents instantaneous axial strain. Once this signal has been generated it can be used for control purposes; the advantages of the diametral strain measurements in this evaluation can be combined with the ability to program and control the axial strain. Figure 6.5 compares the different strain and stress wave forms ob-

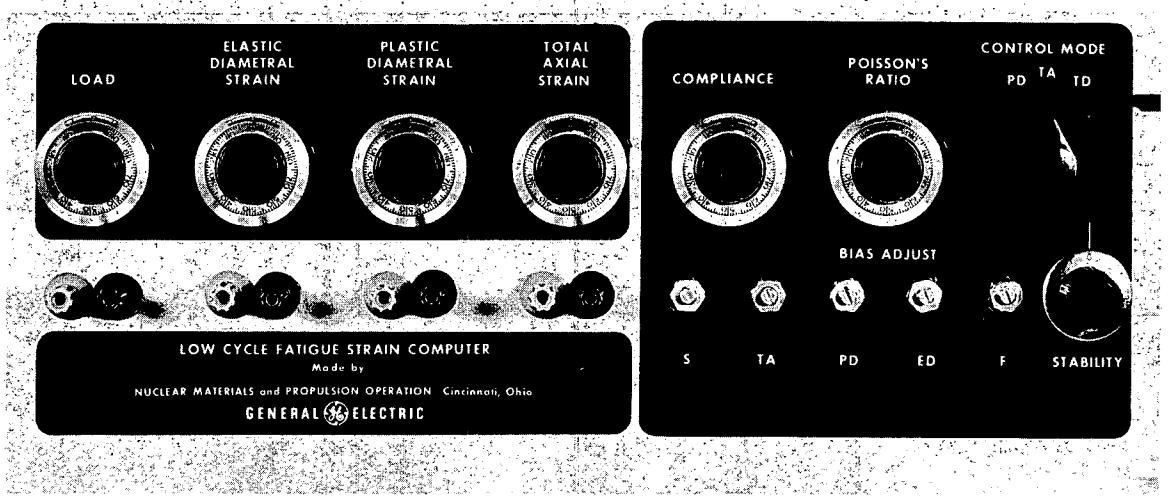

Fig. 6.4 — Front panel of low-cycle fatigue strain computer (Neg. P67-7-32)

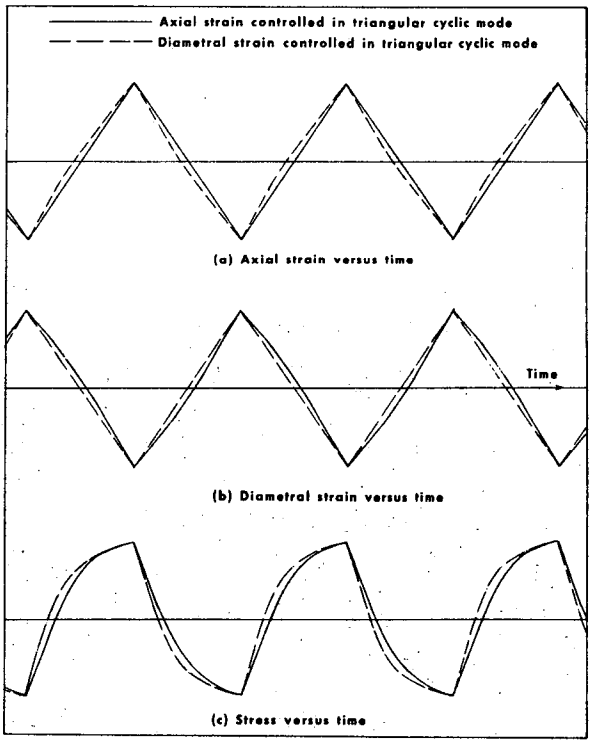

Fig. 6.5 — Comparison of stress and strain wave forms obtained with programming of axial and diametral strain (Type 348 stainless steel at 800°C)

tained[1] in diametral and axial strain control. A triangular wave form (constant strain rate) was programmed in both cases. The strain computer was used to generate the axial strain signal; the diametral strain signal was obtained directly from the diametral extensometer. Such a diagram clearly shows the intra-cycle strain rate differences, but not the more significant, long-term strain reorientation which will change the relationship between axial and diametral strain. For example, the ratio of axial strain range to diametral strain range will increase with cyclic strain hardening and decrease with strain softening. The strain range being controlled, however, will remain at a constant value.

The analog of axial strain is produced by operating upon the signals from the diametral strain extensometer and the load cell. The following relationships form the basis for the axial strain simulation:

$$\epsilon = \epsilon_e + \epsilon_p \tag{6.1}$$

$$\epsilon_e = \frac{-\epsilon_{de}}{\nu_e} \tag{6.2}$$

$$\epsilon_p = \frac{-\epsilon_{dp}}{\nu_p} \tag{6.3}$$

$$\epsilon_{de} = \frac{-F\nu_e}{AE} \tag{6.4}$$

$$\epsilon_{dp} = \epsilon_d - \epsilon_{de} \tag{6.5}$$

where:

ϵ = total axial strain
ϵ_e = elastic axial strain
ϵ_p = plastic axial strain
ϵ_d = total diametral strain
ϵ_{de} = elastic diametral strain
ϵ_{dp} = plastic diametral strain
F = force on the specimen
A = cross sectional area of the specimen at the minimum diameter
ν_e = Poisson's ratio in the elastic region (assumed to be constant)
ν_p = Poisson's ratio in the plastic region (assumed to be 0.5)
E = Young's modulus

Values of A, E, ν_e, and ν_p are readily inserted into the computer as constants, but F and ϵ_d are measured. The other variables are electronically determined using d-c amplifier summing circuits. Sufficient signals are produced to provide the option of programming and controlling diametral strain, axial strain, plastic strain, or force. To calibrate the computer it is necessary only to adjust a potentiometer in the force circuit for zero plastic strain while cycling the specimen in the elastic region. This procedure establishes the ratio ν_e/AE and thus the value of ν_e if E and A are known. The value of ν_e is then set on a front-panel potentiometer dial. When plastic strain control is used it is not necessary to know ν_e or E, since the procedure of adjusting for zero plastic strain in the elastic region defines all necessary relationship.

[1] T. Slot and R. H. Stentz, "Experimental Methods for Low-Cycle Fatigue Research at High Temperature," GE-NMPO, GEMP-527, June 1967.

6.3 TEST RESULTS

During the past year fully reversed strain cycling fatigue data were obtained in an air environment for fully annealed, AISI 348, 304, and 316 stainless steel to determine effects of strain rate, strain range, and temperature. A summary of these data is presented in Tables 6.1, 6.2, and 6.3. As indicated, three strain rates, 4×10^{-3}, 4×10^{-4}, and 4×10^{-5} sec^{-1}, were evaluated at test temperatures of 430°, 650°, and 816°C. Data are also presented for axial strain amplitudes ($\Delta \dot{\epsilon}_t$) ranging from approximately 0.5 to approximately 2.5 percent.

The general effects of strain rate, strain range, and temperature on the cyclic strain fatigue characteristics of 348, 304, and 316 SS are shown graphically in Figures 6.6 through 6.11. Both total axial strain range ($\Delta \dot{\epsilon}_t$) and plastic strain range ($\Delta \epsilon_p$) are presented in terms of N_5, the cycles corresponding to a 5-percent reduction in load. Special tests were performed to identify Poisson' s ratio, employed in conversion[2] from diametral to axial strain, for the 316 SS used in this program. Values for Poisson' s ratio for the 304 and 348 SS have not been obtained yet; hence literature values were employed in the present analysis. This property is being measured for these two materials and any effect which these new data may have on the data presented here will be discussed in a subsequent report. A summary of the short-term tensile data generated to date is presented in Table 6.4.

As indicated in Figures 6.6 and 6.7, the general effect of a decrease in strain rate at 650°C and 816°C results in a severalfold decrease in the fatigue resistance of 348 SS for a given strain ($\Delta \dot{\epsilon}_t$ or $\Delta \epsilon_p$) range. Figure 6.6 also shows that data obtained at 650°C and an axial strain rate of 4×10^{-5} sec^{-1} seem to coincide with data obtained at 816°C and 4×10^{-3} sec^{-1}. The degree of coincidence is reduced, however, if plastic strain range data are used as the basis for the comparison, as shown in Figure 6.7.

Relationships similar to those indicated by the 348 SS data were obtained for the 304 SS as shown in Figure 6.8 and 6.9. The only apparent differences seem to be an increase in slope of the logarithmic plots of plastic strain range versus fatigue life, and slightly lower fatigue resistance for the 304 SS at the same strain levels compared to the 348 SS data. More data are needed for a meaningful interpretation of these slope differences.

Fatigue data for 316 SS are shown in Figures 6.10 and 6.11. The effect of strain rate on fatigue resistance of 316 SS is about the same as that noted for 348 and 304 SS but the temperature effect is quite different. The effect of temperature on the fatigue resistance of 316 SS is much less pronounced than that observed in tests of the other two materials; at the lowest strain rate little, if any, temperature effect on fatigue resistance is noted. This suggests that metallurgical reactions are occurring at 816°C which tend to enhance the fatigue resistance of 316 SS compared to the 650°C results. Another surprising result concerns the lower-than-expected fatigue resistance of the 316 SS at 650°C and the highest strain rate. Metallurgical evaluations are being conducted to identify the mechanisms involved.

The effects of temperature and strain range ($\Delta \dot{\epsilon}_t$ and $\Delta \epsilon_p$) on the fatigue resistance of 316 SS at a constant strain rate of 4×10^{-3} sec^{-1} are shown in Figures 6.12 and 6.13. Based on these limited data, some consistency with the Coffin-Manson relationship, $\Delta \epsilon_p = A N_f^{-m}$, can be identified by the linear isotherms. Although N_5 was used in Figure 6.13, the same general observations follow if N_f is employed. At 430°C the value of m is essentially 0.5 but increases slightly with increasing temperature.

[2] "AEC Fuels and Materials Development Program Progress Report No. 67," GE-NMPO, GEMP-67, June 30, 1967, p. 135.

TABLE 6.1

LOW-CYCLE FATIGUE DATA[a] FOR ANNEALED AISI 348 STAINLESS STEEL TESTED IN AIR AT 650°C AND 816°C

Test Temperature, °C	Specimen No.	Axial Strain: Total Strain Range ($\Delta\dot{\epsilon}_t$), %	Axial Strain: Plastic Strain Range ($\Delta\epsilon_p$), %	Axial Strain: Elastic Strain Range ($\Delta\epsilon_e$), %	Diametral Strain: Total Strain Range ($\Delta\epsilon_d$), %	Diametral Strain: Plastic Strain Range ($\Delta\epsilon_{dp}$), %	Diametral Strain: Elastic Strain Range ($\Delta\epsilon_{de}$), %	Axial Stress: Stress Range at $N_f/2$ ($\Delta\sigma$), kg/mm^2	Cyclic Rate: Frequency of Loading, cycles/sec	Cyclic Rate: Axial Strain Rate, ($\dot{\epsilon}_t$), sec^{-1}	Fatigue Life: Cycles to Fracture (N_f)	Fatigue Life: Cycles to 5% Load Reduction (N_5)	Fatigue Life: Ratio N_5/N_f
650	3-7	2.17	1.79	0.39	1.01	0.89	0.12	56.56	0.001	4.3×10^{-5}	217	193	0.889
	3-6	2.17	1.80	0.37	1.01	0.90	0.11	55.13	0.001	4.3×10^{-5}	208	177	0.851
	3-3	2.18	1.78	0.40	1.01	0.89	0.12	60.86	0.01	4.4×10^{-4}	370	335	0.905
	3-8	2.18	1.78	0.40	1.01	0.89	0.12	60.14	0.01	4.4×10^{-4}	329	320	0.973
	3-5	2.16	1.76	0.40	1.00	0.88	0.12	62.29	0.1	4.3×10^{-3}	550	471	0.856
	3-4	2.19	1.78	0.41	1.01	0.89	0.12	62.29	0.1	4.4×10^{-3}	596	585	0.982
	4-12	1.13	0.80	0.33	0.50	0.40	0.10	47.25	0.002	4.5×10^{-5}	871	760	0.872
	4-10	1.13	0.81	0.32	0.50	0.40	0.10	50.83	0.002	4.5×10^{-5}	950	680	0.716
	4-6	1.12	0.82	0.31	0.50	0.41	0.09	45.11	0.02	4.5×10^{-4}	1259	989	0.786
	4-1	1.13	0.80	0.33	0.50	0.40	0.10	54.41	0.02	4.5×10^{-4}	1360	1133	0.833
	4-9	1.13	0.80	0.33	0.50	0.40	0.10	52.27	0.2	4.5×10^{-3}	2635	2412	0.915
	4-5	1.15	0.78	0.37	0.50	0.39	0.11	51.55	0.2	4.6×10^{-3}	2685	2607	0.971
	3-12	0.61	0.33	0.28	0.25	0.17	0.09	47.61	0.004	4.9×10^{-5}	3661	3236	0.884
	5-12	0.61	0.33	0.28	0.25	0.17	0.09	43.32	0.004	4.9×10^{-5}	7811	5464	0.700
	3-11	0.62	0.30	0.32	0.25	0.15	0.10	45.82	0.04	5.0×10^{-4}	11596	10948	0.944
	9-8	0.62	0.37	0.25	0.26	0.18	0.08	45.82	0.04	5.0×10^{-4}	7807	7269	0.931
	5-3	0.62	0.34	0.27	0.25	0.17	0.08	43.67	0.4	5.0×10^{-3}	15192	15010	0.988
	9-1	0.61	0.34	0.27	0.25	0.17	0.08	43.32	0.4	4.9×10^{-3}	17016	16676	0.980
	9-4	0.62	0.32	0.30	0.25	0.16	0.09	44.25	0.4	5.0×10^{-3}	21432	20652	0.964
816	5-6	2.04	1.94	0.10	1.01	0.97	0.03	22.91	0.001	4.1×10^{-5}	183	118	0.645
	5-7	2.06	1.91	0.15	1.00	0.96	0.04	21.48	0.001	4.1×10^{-5}	233	122	0.524
	5-5	2.11	1.88	0.23	1.01	0.94	0.07	30.06	0.01	4.2×10^{-4}	220	158	0.718
	5-4	2.08	1.88	0.20	1.00	0.94	0.06	30.79	0.01	4.2×10^{-4}	315	176	0.559
	5-1	2.11	1.84	0.27	1.00	0.92	0.08	38.66	0.1	4.2×10^{-3}	317	266	0.839
	6-4	2.09	1.86	0.23	1.00	0.93	0.07	40.09	0.1	4.2×10^{-3}	326	245	0.752
	9-2	1.08	0.91	0.17	0.50	0.45	0.05	20.76	0.002	4.3×10^{-5}	586	385	0.657
	9-5	1.07	0.90	0.17	0.50	0.45	0.05	18.61	0.002	4.3×10^{-5}	582	439	0.754
	9-7	1.09	0.86	0.23	0.50	0.43	0.07	28.64	0.02	4.4×10^{-4}	681	595	0.874
	9-9	1.09	0.86	0.23	0.50	0.43	0.07	28.64	0.02	4.4×10^{-4}	729	462	0.634
	9-6	1.11	0.84	0.27	0.50	0.42	0.08	32.93	0.2	4.4×10^{-3}	1170	746	0.638
	9-11	1.11	0.85	0.25	0.50	0.42	0.08	34.37	0.2	4.3×10^{-3}	949	682	0.719
	6-9	0.55	0.43	0.12	0.25	0.21	0.04	23.27	0.004	4.4×10^{-5}	1862	1554	0.835
	6-10	0.56	0.42	0.14	0.25	0.21	0.04	19.69	0.004	4.5×10^{-5}	1892	1613	0.853
	6-5	0.57	0.40	0.17	0.25	0.20	0.05	23.63	0.04	4.6×10^{-4}	2465	1874	0.760
	6-8	0.58	0.40	0.18	0.25	0.20	0.05	23.63	0.04	4.6×10^{-4}	3160	2718	0.860
	6-3	0.57	0.39	0.17	0.25	0.20	0.05	30.07	0.4	4.6×10^{-3}	4281	3379	0.789
	6-2	0.57	0.39	0.17	0.25	0.20	0.05	32.22	0.4	4.6×10^{-3}	4896	4656	0.951

[a]Control mode: diametral strain.
Strain wave form: triangular with zero mean strain

TABLE 6.2

LOW-CYCLE FATIGUE DATA[a] FOR ANNEALED AISI 304 STAINLESS STEEL TESTED IN AIR AT 650°C AND 816°C

Test Temperature, °C	Specimen No.	Axial Strain			Diametral Strain			Axial Stress	Cyclic Rate		Fatigue Life		
		Total Strain Range ($\Delta\dot{\epsilon}_t$), %	Plastic Strain Range ($\Delta\epsilon_p$), %	Elastic Strain Range ($\Delta\epsilon_e$), %	Total Strain Range ($\Delta\epsilon_d$), %	Plastic Strain Range ($\Delta\epsilon_{dp}$), %	Elastic Strain Range ($\Delta\epsilon_{de}$), %	Stress Range at $N_f/2$ ($\Delta\sigma$), kg/mm^2	Frequency of Loading, cycles/sec	Axial Strain Rate, ($\dot{\epsilon}_t$), sec^{-1}	Cycles to Fracture (N_f)	Cycles to 5% Load Reduction (N_5)	Ratio N_5/N_f
650	10-12	2.12	1.82	0.30	1.00	0.91	0.09	43.67	0.001	4.2×10^{-5}	261	197	0.755
	10-11	2.15	1.78	0.37	1.00	0.89	0.11	52.98	0.01	4.3×10^{-4}	310	287	0.926
	10-9	2.11	1.78	0.33	0.99	0.89	0.10	60.43	0.1	4.2×10^{-3}	566	524	0.925
	10-4	1.11	0.84	0.27	0.50	0.42	0.08	41.53	0.002	4.4×10^{-5}	660	527	0.798
	10-7	1.13	0.81	0.32	0.50	0.41	0.10	46.82	0.02	4.5×10^{-4}	805	748	0.929
	10-10	1.13	0.81	0.32	0.50	0.41	0.10	50.12	0.2	4.5×10^{-3}	1740	1656	0.952
	120	0.58	0.36	0.22	0.25	0.18	0.07	32.84	0.004	4.6×10^{-5}	2134	1533	0.718
	118	0.58	0.38	0.20	0.25	0.19	0.06	33.76	0.004	4.6×10^{-5}	3124	1966	0.629
	296	0.60	0.36	0.24	0.25	0.18	0.07	37.07	0.04	4.8×10^{-4}	3549	3009	0.848
	299	0.61	0.33	0.28	0.25	0.17	0.08	40.38	0.4	4.9×10^{-3}	7320	7100	0.970
	294	0.62	0.32	0.29	0.25	0.16	0.09	41.05	0.4	4.9×10^{-3}	7944	7176	0.903
816	10-2	2.07	1.89	0.18	1.00	0.95	0.06	24.20	0.001	4.1×10^{-5}	130	80	0.615
	7-3	2.07	1.89	0.18	1.00	0.95	0.06	29.35	0.01	4.1×10^{-4}	145	117	0.807
	7-1	2.08	1.88	0.20	1.00	0.94	0.06	34.01	0.1	4.2×10^{-3}	260	226	0.869
	7-12	1.05	0.92	0.13	0.50	0.46	0.04	24.49	0.002	4.2×10^{-5}	307	204	0.664
	7-5	1.07	0.89	0.17	0.50	0.45	0.05	26.92	0.02	4.3×10^{-4}	429	379	0.883
	7-10	1.07	0.89	0.17	0.50	0.45	0.05	32.22	0.2	4.3×10^{-3}	784	529	0.675
	10-3	0.53	0.45	0.09	0.25	0.22	0.03	24.34	0.004	4.2×10^{-5}	788	591	0.750
	7-7	0.54	0.42	0.12	0.25	0.21	0.04	26.49	0.04	4.3×10^{-4}	1338	1055	0.788
	7-9	0.56	0.41	0.15	0.25	0.21	0.05	28.50	0.4	4.5×10^{-3}	2477	2346	0.947

[a]Control mode: diametral strain.

Strain wave form: triangular with zero mean strain.

TABLE 6.3

LOW-CYCLE FATIGUE DATA[a] FOR ANNEALED AISI 316 STAINLESS STEEL TESTED IN AIR AT 430°, 650°, AND 816°C

Test Temperature, °C	Specimen No.	Axial Strain			Diametral Strain			Axial Stress	Cyclic Rate		Fatigue Life		
		Total Strain Range ($\Delta\dot{\epsilon}_t$), %	Plastic Strain Range ($\Delta\epsilon_p$), %	Elastic Strain Range ($\Delta\dot{\epsilon}_e$), %	Total Strain Range ($\Delta\epsilon_d$), %	Plastic Strain Range ($\Delta\epsilon_{dp}$), %	Elastic Strain Range ($\Delta\epsilon_{de}$), %	Stress Range at $N_f/2$ ($\Delta\sigma$), kg/mm^2	Frequency of Loading, cycles/sec	Axial Strain Rate, ($\dot{\epsilon}_t$), sec^{-1}	Cycles to Fracture (N_f)	Cycles to 5% Load Reduction (N_5)	Ratio N_5/N_f
430	14-3	1.85	1.26	0.59	0.81	0.63	0.18	76.07	0.111	4.17×10^{-3}	2202	2161	0.982
	14-4	1.77	1.30	0.47	0.80	0.65	0.15	76.92	0.111	4.03×10^{-3}	1764	1738	0.985
	14-5	1.38	0.91	0.47	0.60	0.45	0.15	63.28	0.148	4.21×10^{-3}	4118	4101	0.996
	14-7	0.91	0.63	0.28	0.40	0.31	0.09	54.91	0.222	4.11×10^{-3}	6325	6094	0.963
	14-6	0.70	0.42	0.28	0.30	0.21	0.09	50.20	0.296	4.34×10^{-3}	21898	21329	0.974
	14-8	0.49	0.24	0.25	0.20	0.12	0.08	49.92	0.444	4.66×10^{-3}	80231	71020	0.885
650	21-8	2.11	1.76	0.35	0.99	0.88	0.11	60.42	0.001	4.22×10^{-5}	98	95	0.969
	16-51	2.16	1.75	0.42	1.00	0.87	0.13	70.59	0.01	4.34×10^{-4}	223	193	0.865
	33-41	1.77	1.32	0.45	0.80	0.66	0.14	74.96	0.111	4.00×10^{-3}	522	496	0.950
	14-2	1.77	1.32	0.45	0.80	0.66	0.14	72.03	0.111	4.00×10^{-3}	553	514	0.929
	14-1	1.37	0.92	0.45	0.60	0.46	0.14	68.81	0.148	4.16×10^{-3}	1032	1006	0.975
	33-42	1.40	0.95	0.45	0.62	0.48	0.14	67.97	0.148	4.24×10^{-3}	1002	980	0.978
	27-17	1.36	0.91	0.45	0.60	0.45	0.14	66.43	0.148	4.13×10^{-3}	945	847	0.896
	16-2	1.11	0.79	0.32	0.50	0.40	0.10	50.82	0.002	4.54×10^{-5}	611	562	0.920
	21-10	1.12	0.77	0.35	0.49	0.39	0.11	58.74	0.02	4.48×10^{-4}	808	764	0.945
	27-2	0.95	0.54	0.41	0.40	0.27	0.13	62.94	0.222	4.39×10^{-3}	2089	1931	0.924
	33-32	0.96	0.55	0.41	0.41	0.27	0.13	61.09	0.222	4.45×10^{-3}	2333	2227	0.954
	27-15	0.74	0.39	0.35	0.30	0.20	0.11	52.73	0.296	4.44×10^{-3}	4304	3961	0.920
	27-18	0.76	0.38	0.38	0.30	0.19	0.12	51.75	0.296	4.56×10^{-3}	4432	4183	0.944
	21-7	0.58	0.36	0.22	0.25	0.18	0.07	42.66	0.004	4.63×10^{-5}	4400	3600	0.818
	16-11	0.60	0.32	0.28	0.25	0.16	0.09	49.34	0.04	4.82×10^{-4}	4490	4208	0.937
	33-33	0.51	0.22	0.29	0.20	0.11	0.09	46.43	0.444	4.80×10^{-3}	11761	11631	0.989
	27-4	0.52	0.23	0.29	0.20	0.11	0.09	46.99	0.444	4.68×10^{-3}	13527	13394	0.990

[a]Control mode: diametral strain.
Strain wave form: triangular with zero mean strain.

TABLE 6.3 (Cont.)

LOW-CYCLE FATIGUE DATA[a] FOR ANNEALED AISI 318 STAINLESS STEEL TESTED IN AIR AT 430°, 650°, AND 816°C

Test Temperature, °C	Specimen No.	Axial Strain: Total Strain Range ($\Delta\dot{\epsilon}_t$), %	Axial Strain: Plastic Strain Range ($\Delta\epsilon_p$), %	Axial Strain: Elastic Strain Range ($\Delta\epsilon_e$), %	Diametral Strain: Total Strain Range ($\Delta\epsilon_d$), %	Diametral Strain: Plastic Strain Range ($\Delta\epsilon_{dp}$), %	Diametral Strain: Elastic Strain Range ($\Delta\epsilon_{de}$), %	Axial Stress: Stress Range at $N_f/2$ ($\Delta\sigma$), kg/mm^2	Cyclic Rate: Frequency of Loading, cycles/sec	Cyclic Rate: Axial Strain Rate, ($\dot{\epsilon}_t$), sec^{-1}	Fatigue Life: Cycles to Fracture (N_f)	Fatigue Life: Cycles to 5% Load Reduction (N_5)	Ratio N_5/N_f
816	21-2	2.04	1.92	0.17	1.00	0.96	0.04	25.31	0.001	4.16×10^{-5}	169	107	0.633
	21-4	2.08	1.87	0.21	0.99	0.94	0.05	28.68	0.001	4.15×10^{-5}	165	131	0.794
	16-9	2.15	1.82	0.33	0.99	0.91	0.08	36.64	0.01	4.30×10^{-4}	270	215	0.796
	21-3	2.14	1.81	0.33	0.99	0.91	0.08	33.03	0.01	4.28×10^{-4}	278	210	0.755
	33-36	1.77	1.44	0.33	0.80	0.72	0.08	43.44	0.111	3.81×10^{-3}	358	291	0.813
	33-37	1.77	1.44	0.33	0.80	0.72	0.08	41.48	0.111	3.81×10^{-3}	398	335	0.842
	27-1	1.37	1.04	0.33	0.60	0.52	0.08	39.82	0.148	3.89×10^{-3}	802	658	0.820
	27-13	1.41	1.04	0.37	0.61	0.52	0.09	37.94	0.148	3.95×10^{-3}	684	628	0.918
	16-1	1.11	0.88	0.23	0.49	0.44	0.05	26.85	0.002	4.42×10^{-5}	497	440	0.885
	14-9	1.12	0.87	0.25	0.49	0.44	0.06	27.97	0.002	4.47×10^{-5}	637	524	0.823
	16-5	1.03	0.76	0.27	0.45	0.38	0.06	35.80	0.02	4.11×10^{-4}	712	547	0.768
	33-39	0.98	0.65	0.33	0.40	0.33	0.08	37.59	0.222	4.03×10^{-3}	1485	1199	0.807
	27-14	0.99	0.66	0.33	0.40	0.33	0.08	36.48	0.222	4.05×10^{-3}	1381	1181	0.855
	27-16	0.72	0.47	0.25	0.30	0.23	0.06	35.08	0.296	4.03×10^{-3}	2406	1933	0.803
	33-40	0.75	0.46	0.29	0.30	0.23	0.07	37.59	0.296	4.13×10^{-3}	1938	1742	0.899
	16-10	0.59	0.39	0.21	0.24	0.19	0.05	25.17	0.004	4.72×10^{-5}	1832	1530	0.835
	21-5	0.60	0.39	0.21	0.25	0.20	0.05	25.06	0.004	4.79×10^{-5}	2006	1600	0.797
	16-8	0.61	0.39	0.22	0.25	0.20	0.05	32.45	0.04	4.85×10^{-4}	2121	1718	0.810
	33-35	0.54	0.29	0.25	0.20	0.14	0.06	30.63	0.444	4.29×10^{-3}	6443	5984	0.929
	27-12	0.58	0.29	0.29	0.21	0.14	0.07	32.02	0.444	4.57×10^{-3}	4961	4375	0.882

[a]Control mode: diametral strain

Strain wave.form: triangular with zero mean strain

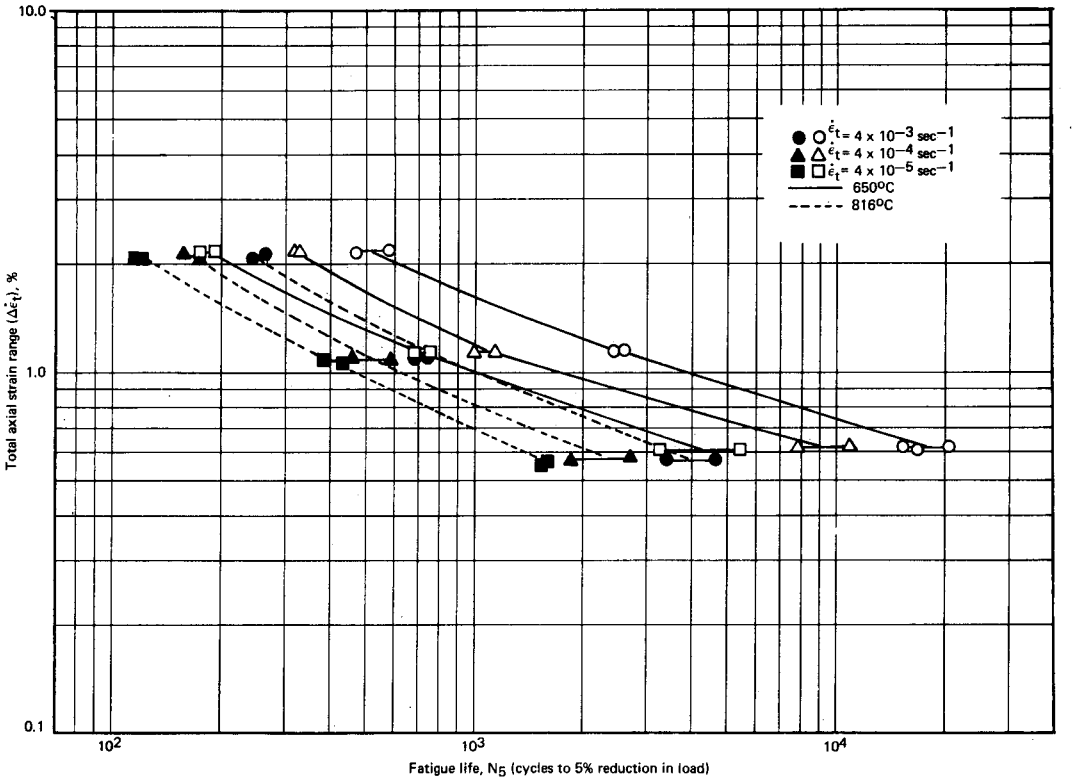

Fig. 6.6 – Total axial strain range versus fatigue life (N_5) for AISI 348 stainless steel tested in air

A comparison of plastic strain fatigue characteristics of 348, 304, and 316 SS obtained at 430°, 650°, and 816°C and a strain rate of 4×10^{-3} sec^{-1} is shown in Figures 6.14, 6.15, and 6.16. At 430°C[3] the 316 SS is slightly less fatigue resistant than the 348 SS. No data have been obtained for 304 SS at this temperature. At 650°C the 316 SS is considerably less fatigue resistant than the 348 SS and slightly less than the 304 SS. Based on the data at 816°C, the 348 and 316 SS exhibit similar fatigue characteristics for a given strain level, whereas 304 SS is slightly less fatigue resistant than either of these two materials over the strain range evaluated.

Plots of stress range versus total axial strain range for 316 SS at 650°C and 816°C and for a constant strain rate of 4×10^{-3} sec^{-1} are shown in Figure 6.17. The stress values represent steady-state stress range data and were usually obtained at $N_f/2$. In general, 316 SS data for 650°C and 816°C exhibited cyclic hardening followed by the steady-state stress range indicated in Tables 6.1, 6.2, and 6.3. At 430°C, however, it exhibited cyclic hardening followed by cyclic softening; this phenomenon was observed over the entire strain range evaluated, as shown in Figure 6.18. In this evaluation, axial strain range data were calculated from diametral strain measurements obtained at the steady-state stress range which occurred after most cyclic hardening or cyclic softening had been completed.

6.4 FATIGUE DATA ANALYSIS

An analysis of fatigue data generated to date on 304, 348, and 316 SS at 650°C and 816°C for an approximate axial strain rate of 4×10^{-3} sec^{-1} is shown in Figures 6.19 through

[3]"AEC Fuels and Materials Development Program Progress Report No. 71," GE-NMPO, GEMP-1002, December 29, 1967, p. 96.

TABLE 6.4

SUMMARY OF SHORT-TERM TENSILE DATA FOR AISI TYPES 348, 304, AND 316 STAINLESS STEEL

Fully Annealed Stainless Steel	Test Temperature, °C	Young's Modulus (E), 10^3 kg/mm^2	Axial Strain Rate ($\dot{\epsilon}_t$), sec^{-1}	Reduction in Area, %	Poisson's Ratio (elastic), ν_e
AISI 316	20	21.16	4×10^{-3}	[a]	[a]
	430	16.87	4×10^{-3}	60.0	0.32
	430	16.87	4×10^{-5}	57.1	0.32
	650	15.43	4×10^{-3}	60.4	0.31
	650	15.43	4×10^{-5}	33.4	0.31
	816	12.94	4×10^{-3}	56.5	0.26
	816	12.94	4×10^{-5}	49.8	0.26
AISI 304	20	20.18	4×10^{-3}		0.3[b]
	20	20.18	4×10^{-5}		
	430	16.45	4×10^{-3}		0.3[b]
	430	16.45	4×10^{-5}		
	650	15.19	4×10^{-3}		0.3[b]
	650	15.19	4×10^{-5}		
	816	[a]	[a]		0.3[b]
AISI 348	20	19.82	4×10^{-3}	[a]	0.3[b]
	20	19.82	4×10^{-5}		
	430	16.73	4×10^{-3}		0.3[b]
	430	16.73	4×10^{-5}		
	650	15.33	4×10^{-3}		0.3[b]
	650	15.33	4×10^{-5}		
	816	13.39	4×10^{-3}		0.3[b]
	816	13.39	4×10^{-5}		

[a]Values are being determined.
[b]Assumed values.
Poisson's Ratio (plastic) = 0.5.

6.24. In this analysis, the Manson-Halford[4] approach was employed to predict low-cycle fatigue behavior. These calculations followed from the expression:

$$\Delta\dot{\epsilon}_t = \frac{3.5\,\sigma_u}{E} N_f^{-0.12} + D^{0.6}\, N_f^{-0.6} \qquad (6.6)$$

where:

σ_u is the ultimate tensile strength
E is the modulus of elasticity
D is $\ln \frac{1}{1-RA}$
RA is reduction in area expressed as a fraction
N_f is the number of cycles to failure

Using the short-term tensile data presented in Table 6.5, the N_f values corresponding to assumed $\Delta\dot{\epsilon}_t$ values were calculated. Based on the Manson-Halford suggestions, the lower-, average-, and upper-bound curves were positioned.

The short-term tensile property data and Poisson's Ratio needed for the conversion of diametral strain to axial strain are handbook values; hence the correlation obtained should be considered preliminary. Short-term tensile data and values for Poisson's Ratio are being generated for the alloys under investigation to secure a better correlation. As shown in Figures 6.19 through 6.24, data for the three alloys evaluated generally lie near the

[4]S. S. Manson and G. Halford, "A Method of Estimating High-Temperature Low-Cycle Fatigue Behavior of Metals," NASA TM X-52270, 1967.

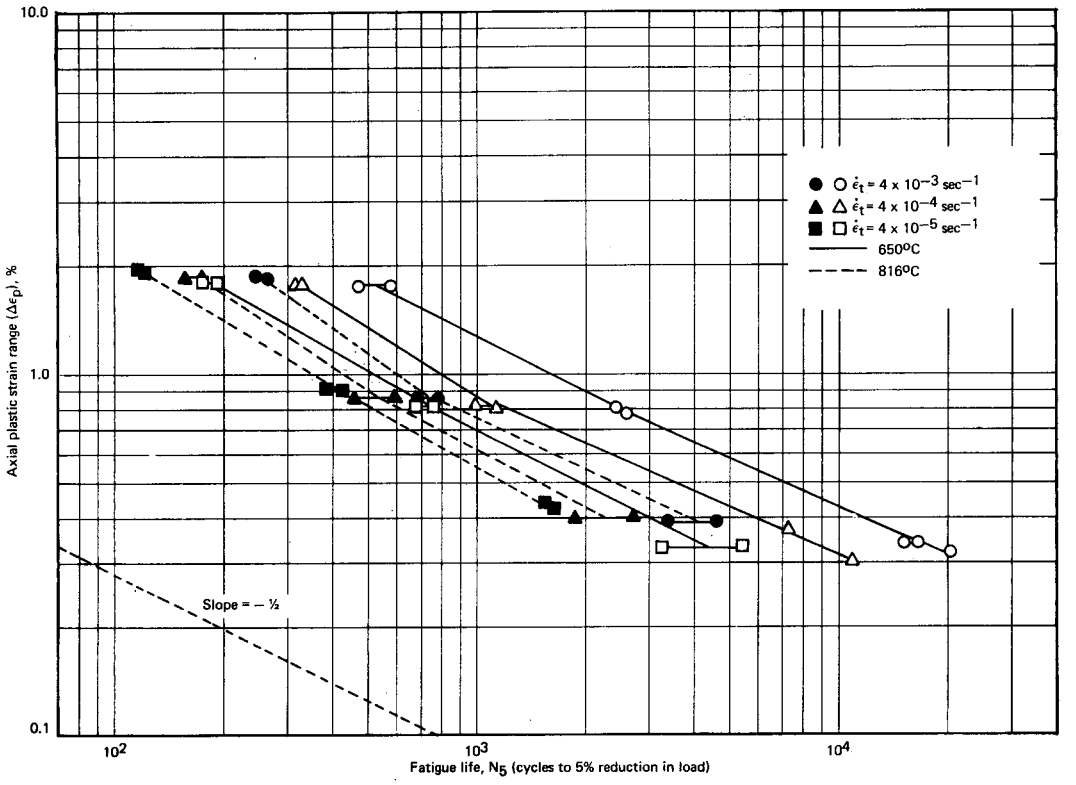

Fig. 6.7 – Axial plastic strain range versus fatigue life (N_5) for AISI 348 stainless steel tested in air

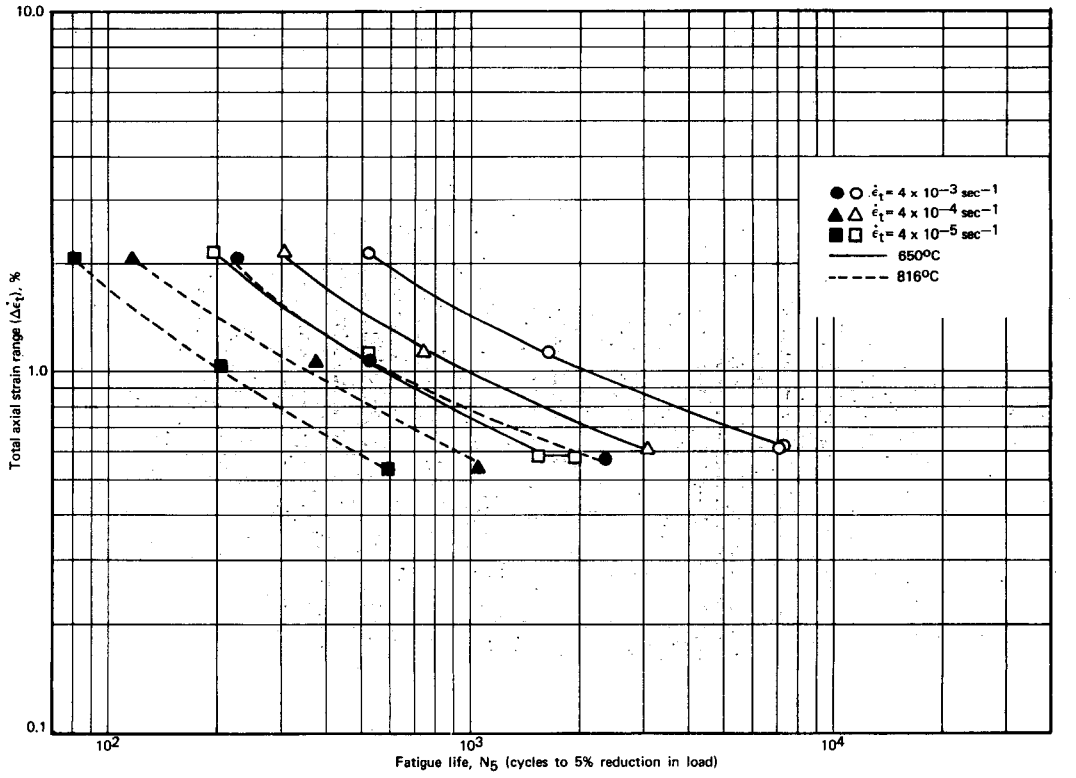

Fig. 6.8 – Total axial strain range versus fatigue life (N_5) for AISI 304 stainless steel tested in air

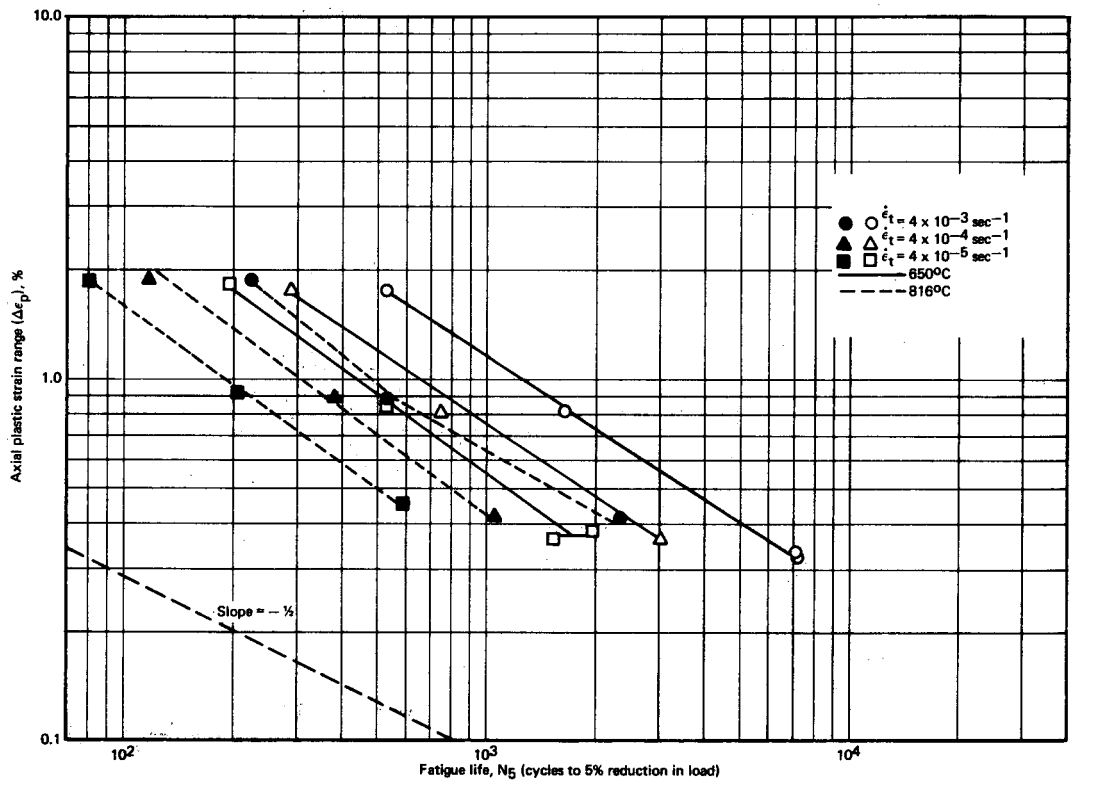

Fig. 6.9 – Axial plastic strain range versus fatigue life (N_5) for AISI 304 stainless steel tested in air

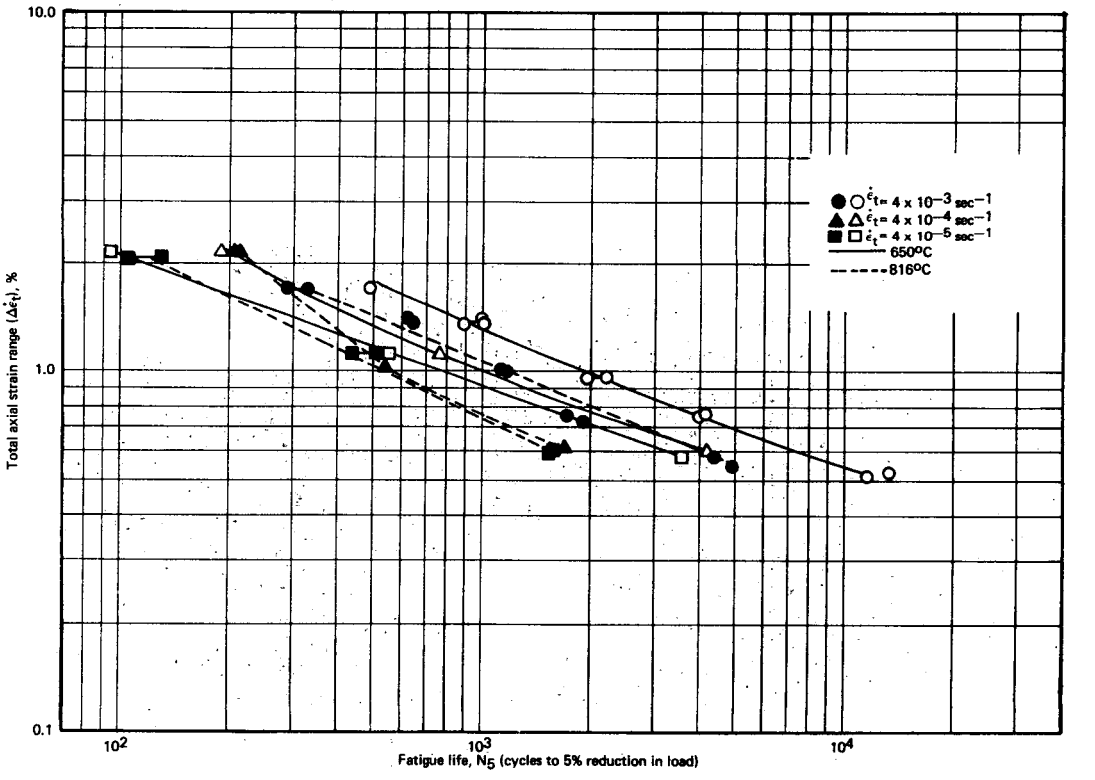

Fig. 6.10 – Total axial strain range versus fatigue life (N_5) for AISI 316 stainless steel tested in air

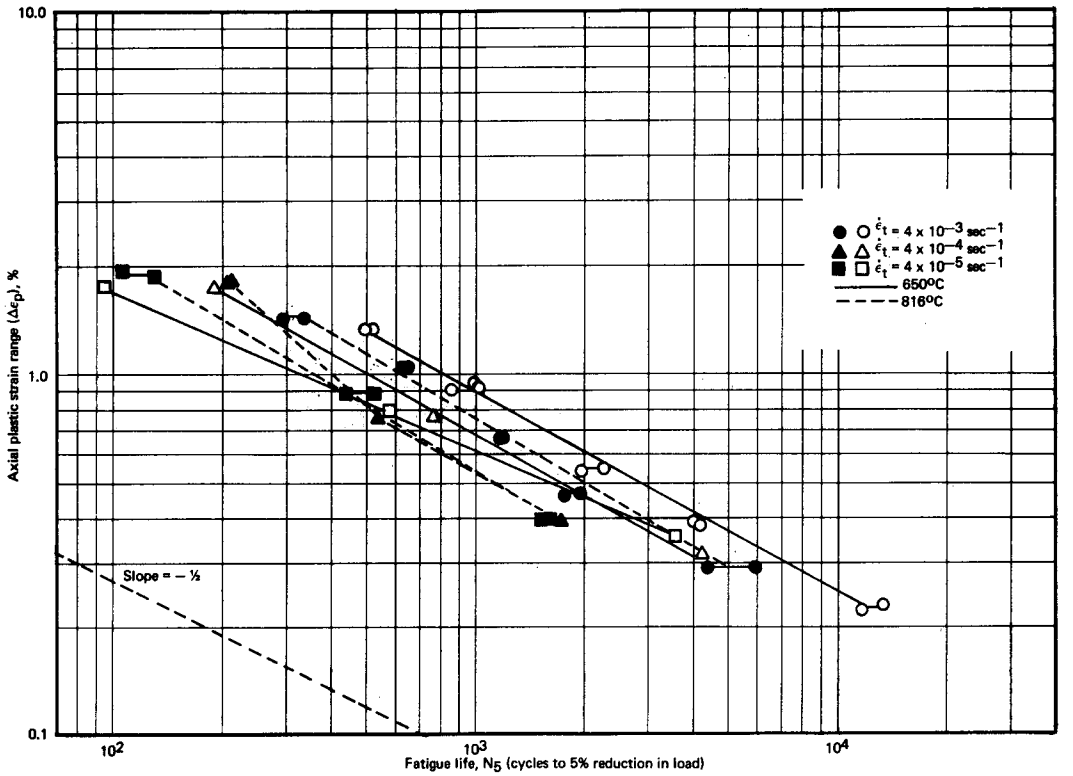

Fig. 6.11 – Axial plastic strain range versus fatigue life (N_5) for AISI 316 stainless steel tested in air

upper-bound of the predicted curve, except for the 348 SS data at 816°C. Data in the high-life region ($\Delta\dot{\epsilon}_t \sim 0.5\%$) for both 650°C and 816°C become more conservative than those predicted for the upper-bound limit using the expression mentioned. Work will continue using the short-term property data characteristic of the material being evaluated. Additional correlations that include the lower strain rate data will also be evaluated.

In all evaluations mentioned above, two definitions of fatigue life were encountered. In addition to the number of cycles to failure, N_f, the number of cycles to a 5-percent reduction in load, N_5, was employed. A comparison of N_5 to N_f is presented in Tables 6.1, 6.2, and 6.3. Since N_5 corresponds to a fairly significant drop in the load, this point is expected to occur near the failure point. For this reason the ratio N_5/N_f should be a fraction closer to unity than to zero. If a value of 0.75 is selected, data in Tables 6.1, 6.2, and 6.3 indicate only 16 of 99 data points with N_5/N_f values below 0.75. Other interesting data obtained in this evaluation are:

1. Only 1 of 42 data points for 316 SS has a ratio of N_5/N_f below 0.75; this compares to 5 of 20 for 304 SS and 10 of 37 for 348 SS. Obviously for the 316 SS fracture is closer at hand when the N_5 point is reached.
2. Ranges of the N_5/N_f values are:
   0.524 to 0.988 for 348 SS
   0.615 to 0.970 for 304 SS
   0.633 to 0.996 for 316 SS.
3. Twelve of the 16 N_5/N_f values below 0.75 correspond to tests at 816°C.
4. Only two of the 16 N_5/N_f values below 0.75 were obtained in tests at a strain rate of 4×10^{-3} sec^{-1}.
5. Only three of the 16 N_5/N_f values below 0.75 correspond to strain range tests below 1 percent.

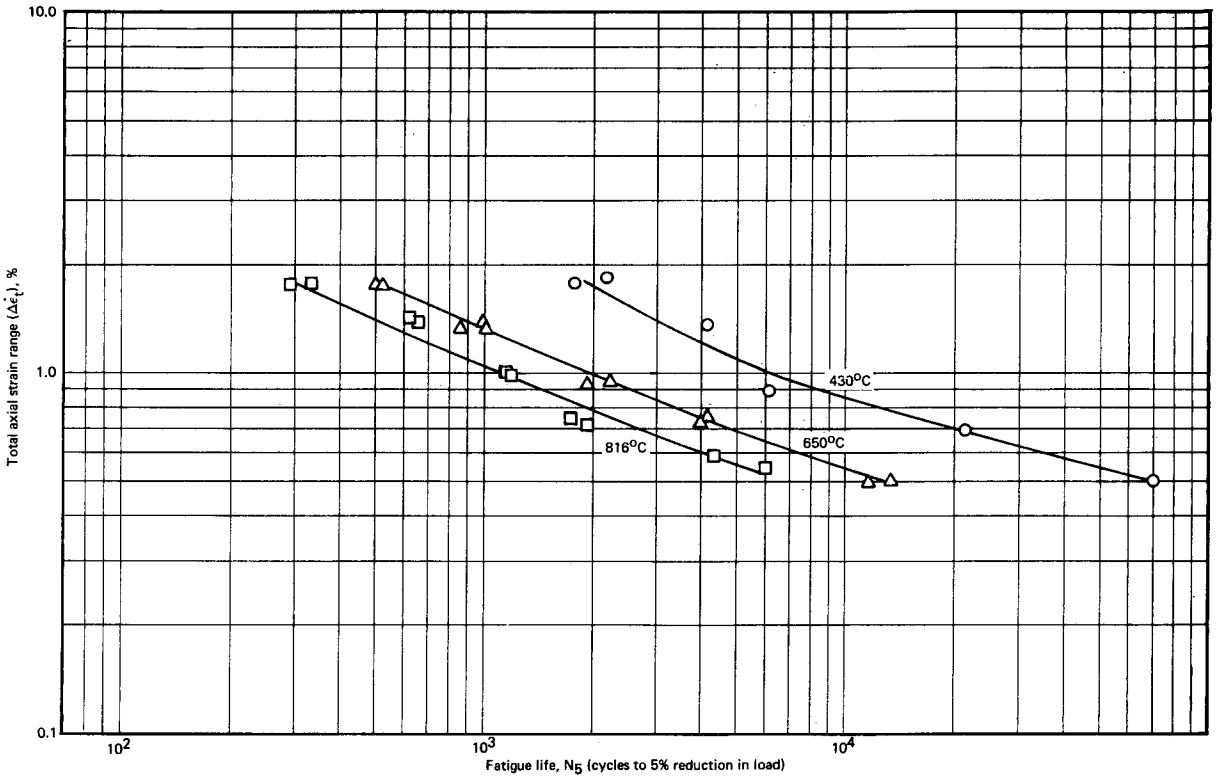

Fig. 6.12 – Total axial strain range versus fatigue life (N_5) for AISI 316 stainless steel tested in air; axial strain rate $\Delta\dot{\epsilon}_t = 4 \times 10^{-3}$ sec^{-1}

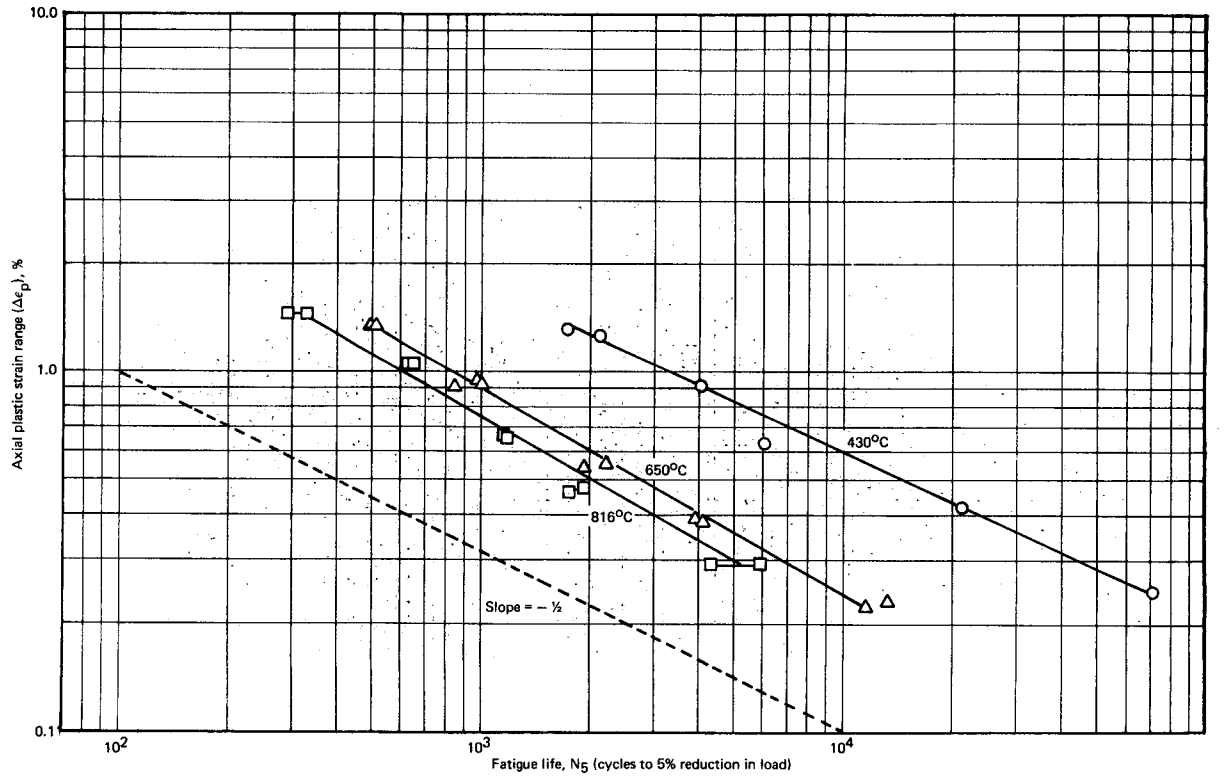

Fig. 6.13 – Axial plastic strain range versus fatigue life (N_5) for AISI 316 stainless steel tested in air; axial strain rate $\dot{\epsilon}_t = 4 \times 10^{-3}$ sec^{-1}

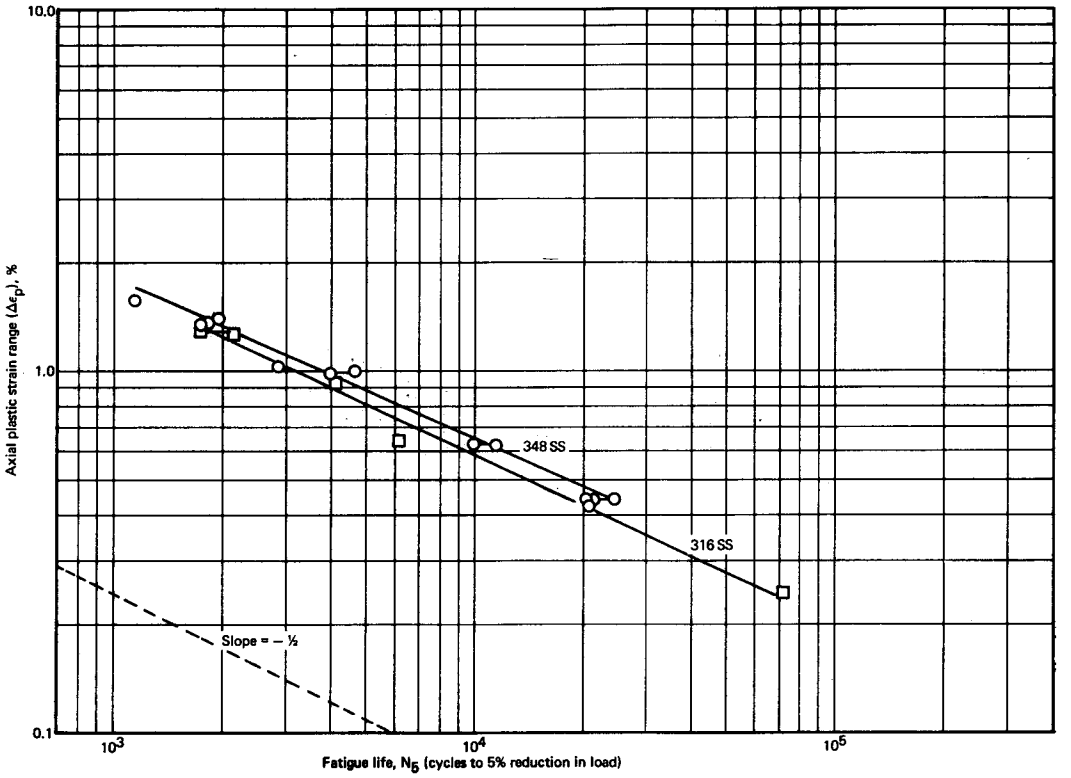

Fig. 6.14 – Axial plastic strain range versus fatigue life (N_5) for AISI 316 and 348 stainless steel at 430°C and an axial strain rate of 4×10^{-3} sec^{-1}

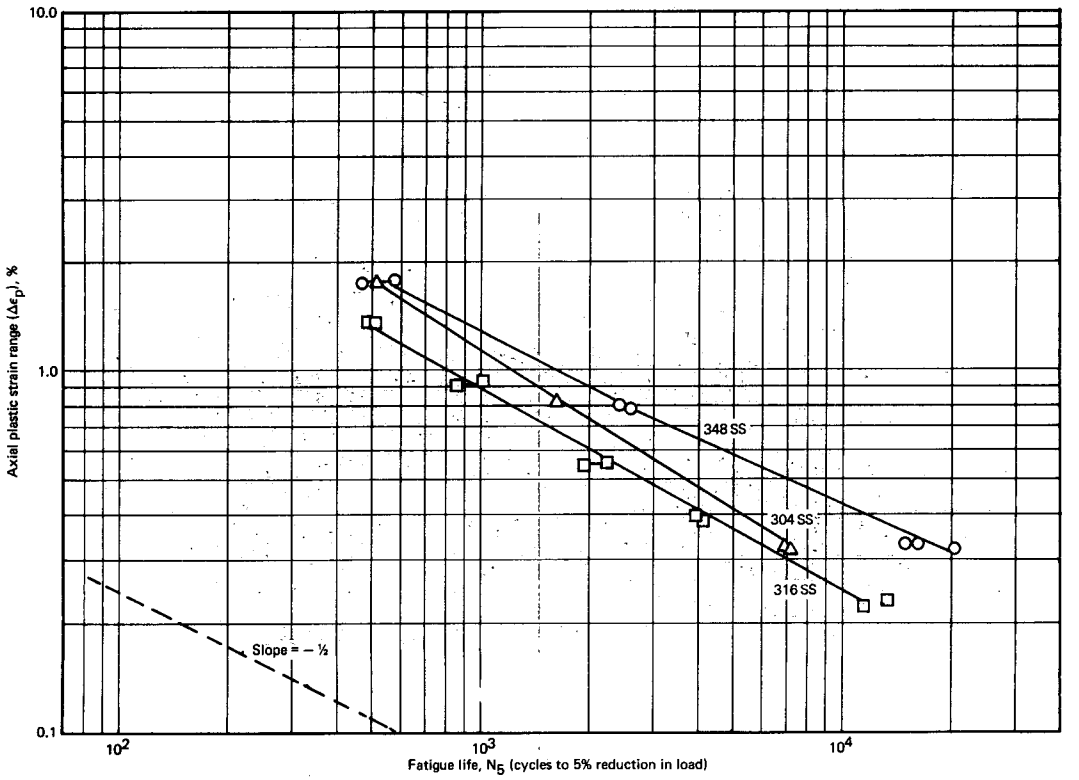

Fig. 6.15 – Axial plastic strain range versus fatigue life (N_5) for AISI 304, 316, and 348 stainless steel at 650°C and an axial strain rate of 4×10^{-3} sec^{-1}

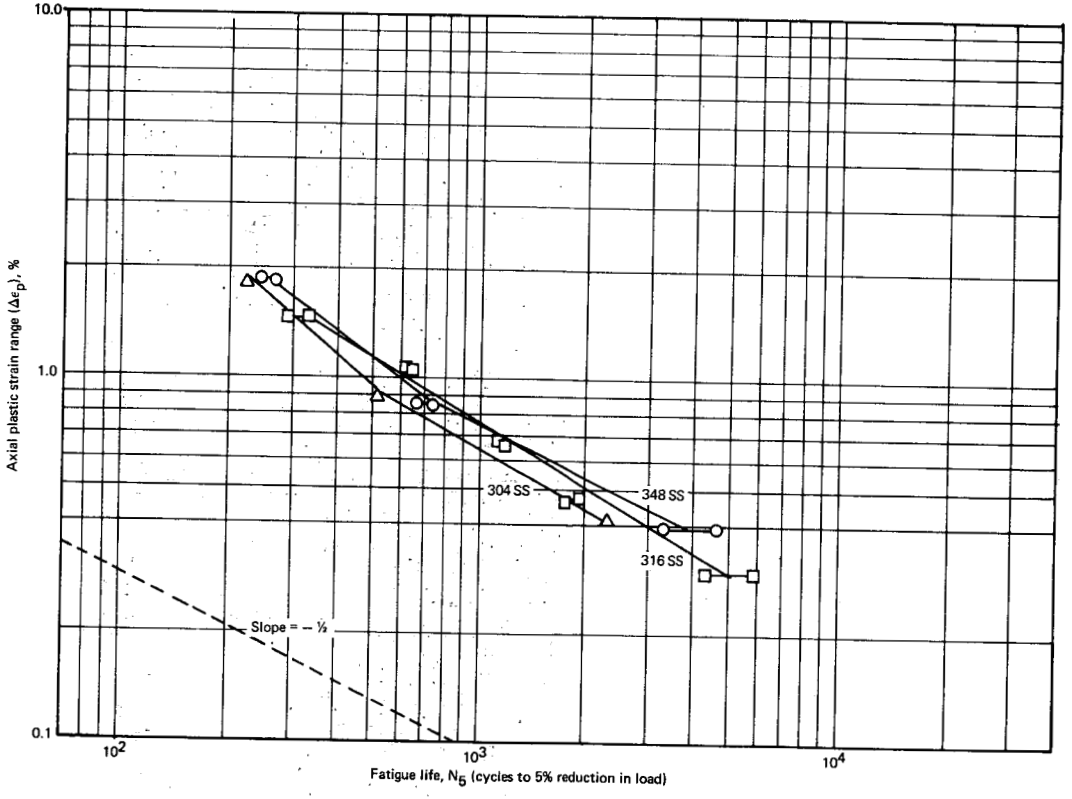

Fig. 6.16 – Axial plastic strain range versus fatigue life (N_5) for AISI 304, 316, and 348 stainless steel at 816°C and an axial strain rate of 4×10^{-3} sec^{-1}

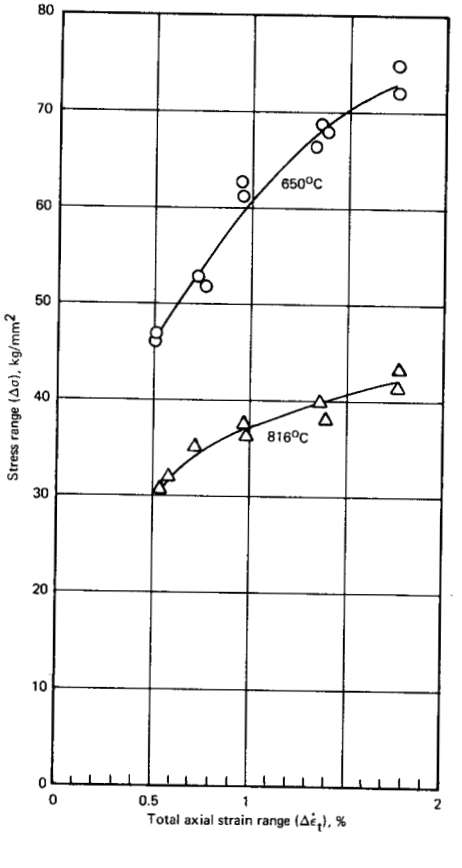

Fig. 6.17 – Stress range versus total axial strain range for AISI 316 stainless steel at a strain rate of 4×10^{-3} sec^{-1}

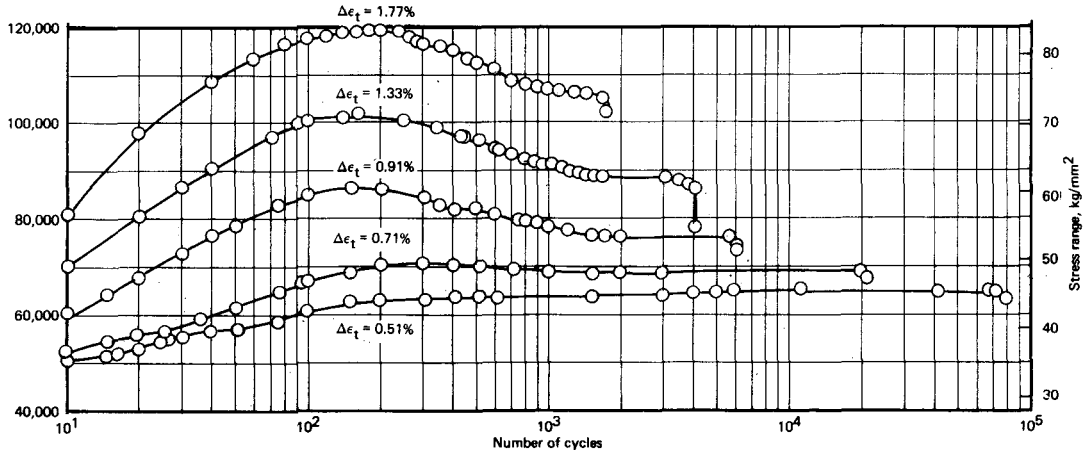

Stress range versus cycles obtained for AISI 316 stainless steel at 430°C with an axial strain rate of 4×10^{-3} sec^{-1}

Fig. 6.18 – Stress range versus cycles for AISI 316 stainless steel at 430°C and an axial strain rate of 4×10^{-3} sec^{-1}

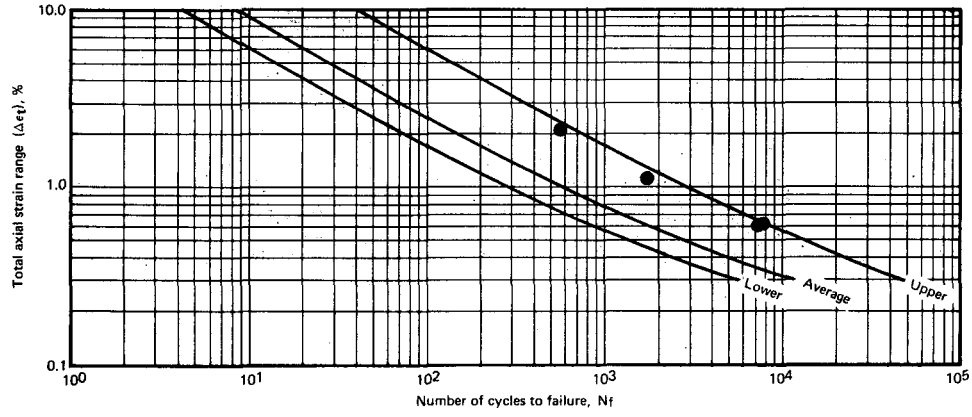

Fig. 6.19 – Correlation of high-temperature fatigue data obtained for AISI 304 stainless steel at 650°C and a constant strain rate of ~4×10^{-3} sec^{-1}

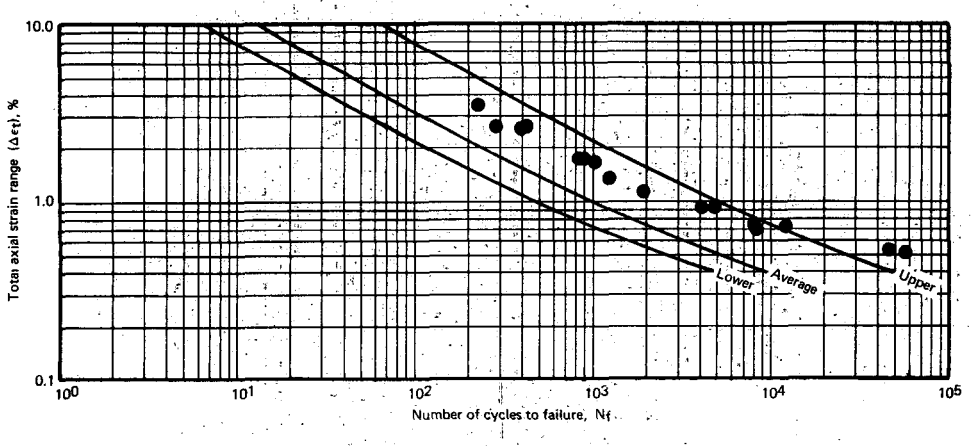

Fig. 6.20 – Correlation of high-temperature fatigue data obtained for AISI 348 stainless steel at 650°C and a constant strain rate of ~4×10^{-3} sec^{-1}

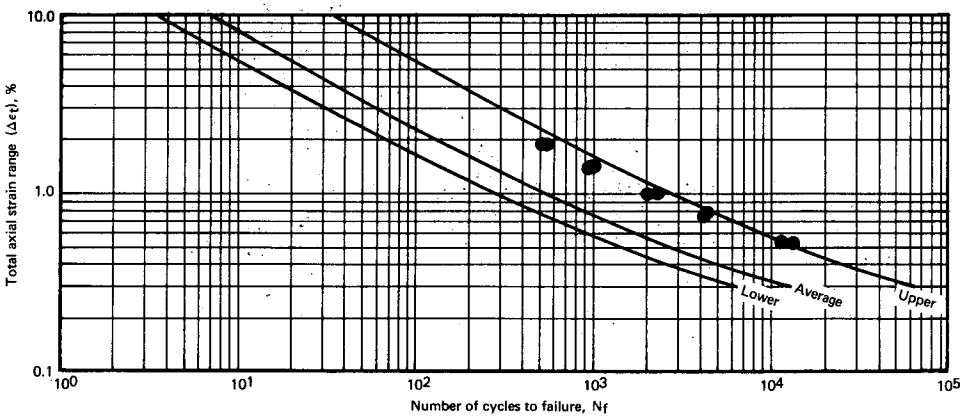

Fig. 6.21 — Correlation of high-temperature fatigue data obtained for AISI 316 stainless steel at 650°C and a constant strain rate of ~4 x 10^{-3} sec^{-1}

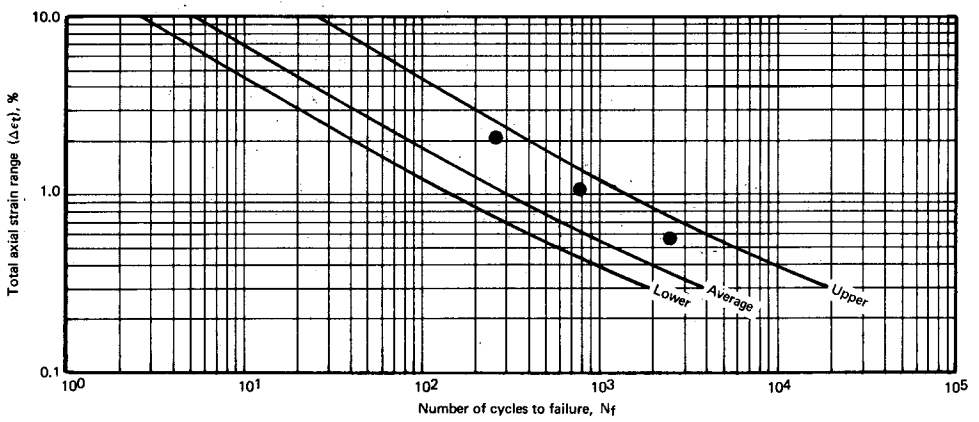

Fig. 6.22 — Correlation of high-temperature fatigue data obtained for AISI 304 stainless steel at 816°C and a constant strain rate of ~4 x 10^{-3} sec^{-1}

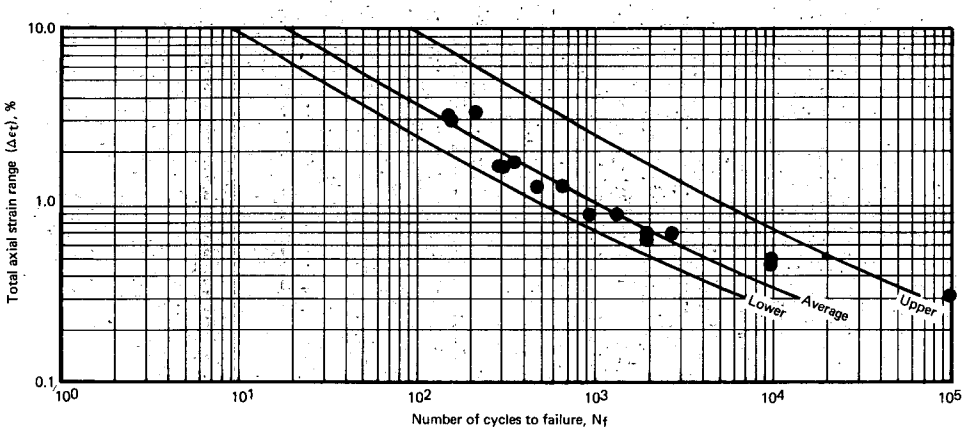

Fig. 6.23 — Correlation of high-temperature fatigue data obtained for AISI 348 stainless steel at 816°C and a constant strain rate of ~4 x 10^{-3} sec^{-1}

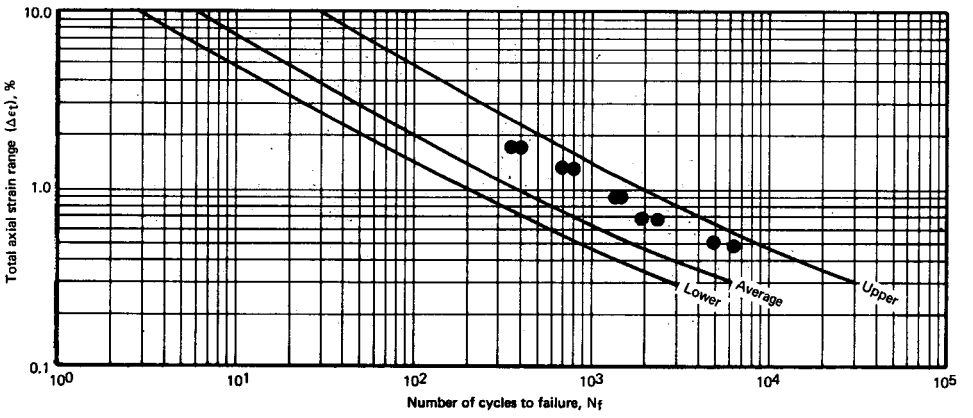

Fig. 6.24 – Correlation of high-temperature fatigue data obtained for AISI 316 stainless steel at 816°C and a constant strain rate of $\sim 4 \times 10^{-3}$ sec^{-1}

TABLE 6.5

SHORT-TERM TENSILE DATA[a] FOR CORRELATION OF HIGH-TEMPERATURE FATIGUE RESULTS OBTAINED FOR AISI 304, 348, AND 316 STAINLESS STEEL

Material	Temperature, °C	Ultimate Tensile Strength, kg/cm^2	Young's Modulus, kg/cm^2 x 10^{-6}	D[b]
304	650	2882	1.546	0.867
348	650	3233	1.398	1.295
316	650	3093	1.476	0.756
304	816	1406	1.335	0.545
348	816	1575	1.272	1.87
316	816	2039	1.335	0.60

[a]Literature data.

[b]D is $\ln \frac{1}{1 - RA}$

6. Only three of the 16 N_5/N_f values below 0.75 correspond to frequencies above 0.01 sec^{-1}.

Although no detailed study has been made of this relationship, attention has been focused recently on evaluating the condition of the specimen at the N_5 point. Visual observations during test have shown that the specimen is definitely cracked at this point but no quantitative data were available to define the extent of cracking. Post-test metallographic evaluations have been initiated in an attempt to acquire more specific information relating to crack initiation and propagation. A fractographic analysis based on both light and electron microscopy has been made to yield measurements of the fatigue striations. These data were used to plot crack length as a function of the number of fatigue cycles. In the two plots obtained to date (Figure 6.25), the measured N_5 point was found to correspond to a crack length of about 1.7 mm. As this study continues, some indication should be obtained of the crack initiation point or of the crack length, where the demand strain remains fairly uniform over the controlled cross section.

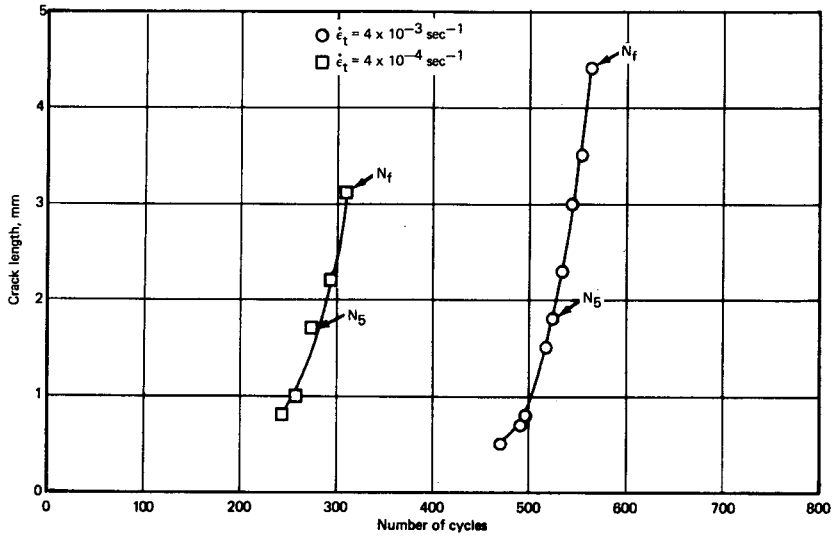

Fig. 6.25 — Relationship of fatigue cycles to crack length for AISI 304 stainless steel tested in air at 650°C; $\Delta\dot{\epsilon}_t = 2.1\%$

6.5 METALLOGRAPHIC AND FRACTOGRAPHIC ANALYSIS OF LOW-CYCLE FATIGUE SPECIMENS

Post-test metallographic and fractographic analyses of low-cycle fatigue specimens were initiated. Information obtained in this study is expected to provide some understanding of behavior observed in the experimental fatigue testing program, and of basic mechanisms involved in crack initiation, crack propagation, and fracture phases of metal fatigue.

Standard metallographic techniques described previously,[5] were used to characterize the fracture mode of AISI 304 and 348 stainless steel as a function of strain rate, strain range, and temperature. The specimens were sectioned longitudinally through the area where both the initial and final fracture occurred, and this cross section was prepared for metallographic evaluation. Photomicrographs of the structure of these two materials in the pre-test condition are shown in Figures 6.26 and 6.27. AISI 304 SS had a uniform equiaxed grain structure with twins in some grains and an ASTM grain size of 2 to 3. AISI 348 SS had a duplex grain structure with a fine-grained center surrounded by a coarse-grained outer layer. The fine-grained portion varied from one fatigue specimen to another. Because of this duplex structure, two ASTM grain sizes are reported: fine-grained material 10, and coarse-grained material 4 to 5.

Metallographic analyses were made of the cross sections of the fractures of 304 SS tested at 650°C, at two strain ranges (2 and 0.6%), and at three strain rates (4×10^{-5}, $\times 10^{-4}$, and $\times 10^{-3}$ sec^{-1}). The crack initiated and propagated transgranularly in the specimens tested at the highest strain rate at both strain ranges. In specimens tested at the lower strain rates, the cracks initiated intergranularly and propagated both trans- and intergranularly. At the final fracture in all specimens, the grains were elongated and cracks appeared on the outer surfaces. Metallographic examination revealed a grain boundary phase in all fatigue specimens. Etch pits were seen in the highly stressed areas, indicating the dislocations which formed in the stressed metal.

AISI 304 SS specimens tested at 816°C, at two different strain ranges, and at three different strain rates were also analyzed. In these specimens the crack initiated and propa-

[5]GEMP-1002, pp. 102–105.

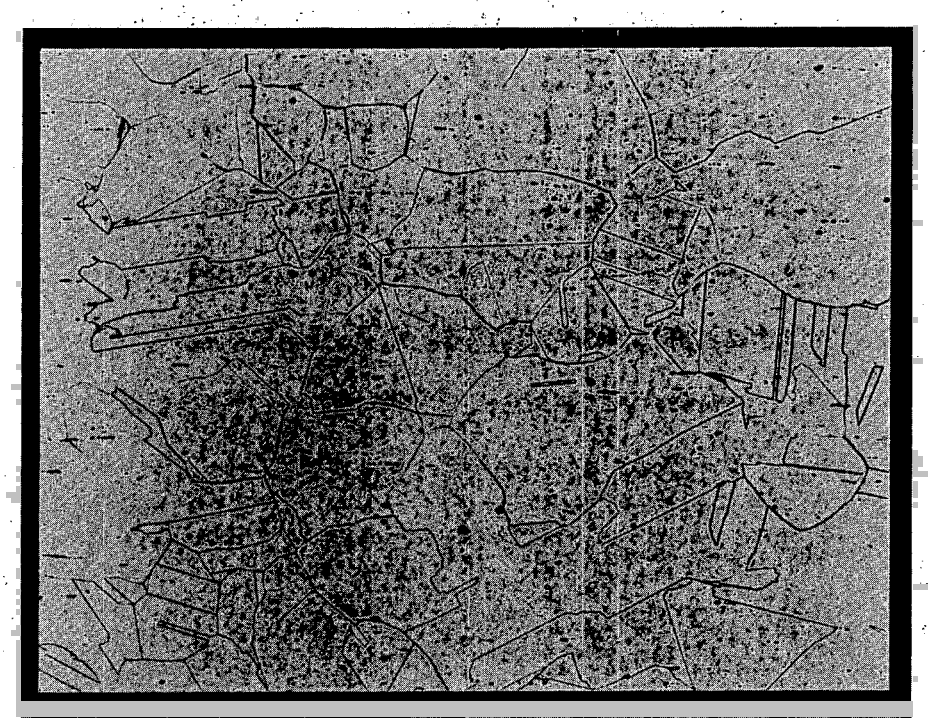

Fig. 6.26 – Photomicrograph showing pre-test structure of AISI 304 stainless steel (longitudinal cross section) used in low-cycle fatigue testing. (Neg. 10282; $22H_2SO_4$, $12H_2O_2$ [30%], $66H_2O$, electrolytic etchant; 100X)

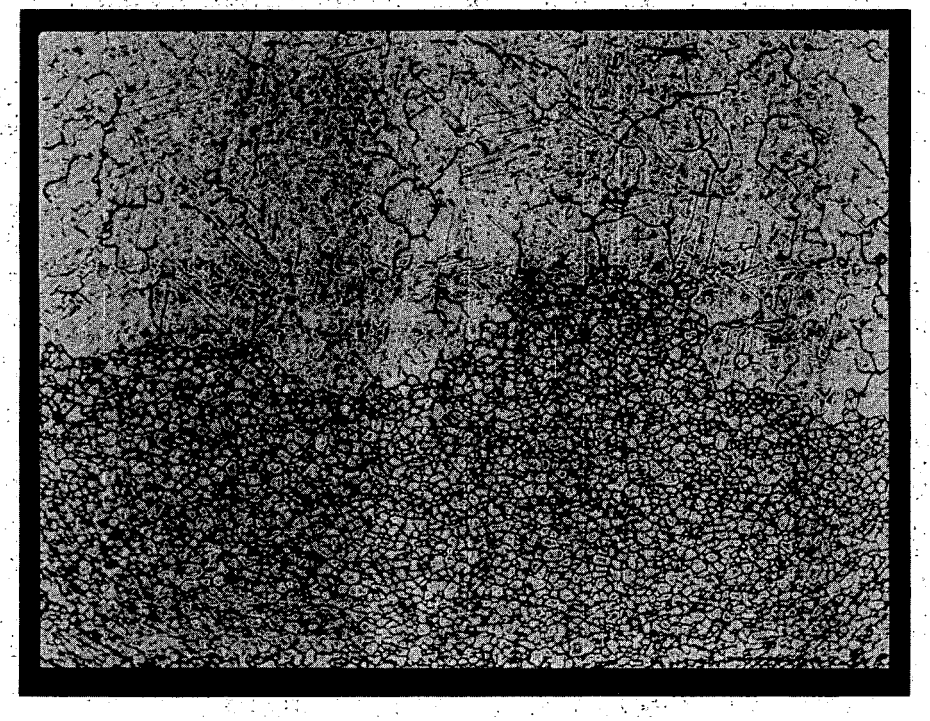

Fig. 6.27 – Photomicrograph showing pre-test structure of AISI 348 stainless steel (longitudinal cross section) used in low-cycle fatigue testing. (Neg. 10281; $50HNO_3$, $50H_2O$, electrolytic etchant; 100X)

gated intergranularly; at the final fracture the grains were elongated. In the highly strained regions of the 2-percent strain range specimens, subgrains were observed at the lowest strain rate, subgrains and etch pits at the intermediate strain rate, and etch pits at the highest strain rate. In the highly strained regions of the 0.6-percent strain range specimens, no etch pits or subgrains were observed at the lowest strain rate; at the intermediate strain rate etch pits were observed, and at the highest strain rate subgrains appeared. At the lowest strain rate the grain boundary phase was intermittent; at the highest strain rates it was continuous (see Figure 6.28).

Post-test metallographic analyses were performed on AISI 348 SS specimens tested at two temperatures, three strain rates, and two strain ranges. As stated previously, this material had a duplex grain structure, and the amount of fine-grained material varied from specimen to specimen. There was no change in the grain boundary phase in this material, as was seen in the 304 SS. In each specimen the crack initiated intergranularly in the large-grained areas and propagated transgranularly. Numerous secondary cracks occurred on the outer periphery of the specimens tested at the 2-percent strain range at both temperatures, but at the 0.6-percent strain range, only a few small secondary cracks appeared. The fractures varied considerably, depending upon the strain range. At the lowest strain range fractures were almost straight across except where the final separation took place (compare Figures 6.29 and 6.30). Another difference appeared in the fatigue specimens tested at 816°C at the lowest strain range; a series of cracks developed at an angle approximately 60 degrees to the fractured surface in the direction the crack was propagating (see Figure 6.31). Indications of this condition appeared in other tests but they were not nearly so pronounced.

Results of metallographic analyses of 304 and 348 SS specimens are summarized in Table 6.6.

To characterize the AISI 316 SS for the low-cycle fatigue program, longitudinal and transverse cross sections were prepared for metallographic analyses. The analysis and pre-test processing were reported previously.[6] No differences were noted in the two cross sections, and the material had been fully recrystallized with a uniform equiaxed grain structure (Figure 6.32); ASTM grain size was 4 to 5. Twins were noted in some of the grains.

To study the fractured surfaces of low-cycle fatigue specimens at higher magnification, techniques were developed for replicating the area of interest for study in the electron microscope.[7] These procedures are used extensively. Each striation on the fractured surface (Figure 6.33) is the result of one cycle in the fatigue test. A study is in progress to correlate this striation density with strain rate, strain range, and temperature of materials being tested. Striations could not be resolved at 1500X at the crack initiation point for the 304 SS tested at the lowest strain rate ($\sim 4 \times 10^{-5}$ sec^{-1}), and a strain range of 2 percent. This is apparently due to the low strain rate imposed during testing. In the 304 SS tested at 650°C, 2-percent strain range, and at the two highest strain rates, the cracks had propagated approximately 30 percent of the diameter (~2 mm) of the test specimen at the N_5 point.

6.6 SUMMARY AND CONCLUSIONS

Several modifications incorporated in the four low-cycle fatigue systems this year improved strain programming versatility, load measurement sensitivity, and strain calibration accuracy.

[6] GEMP-1002, p. 94.

[7] GEMP-1002, p. 105.

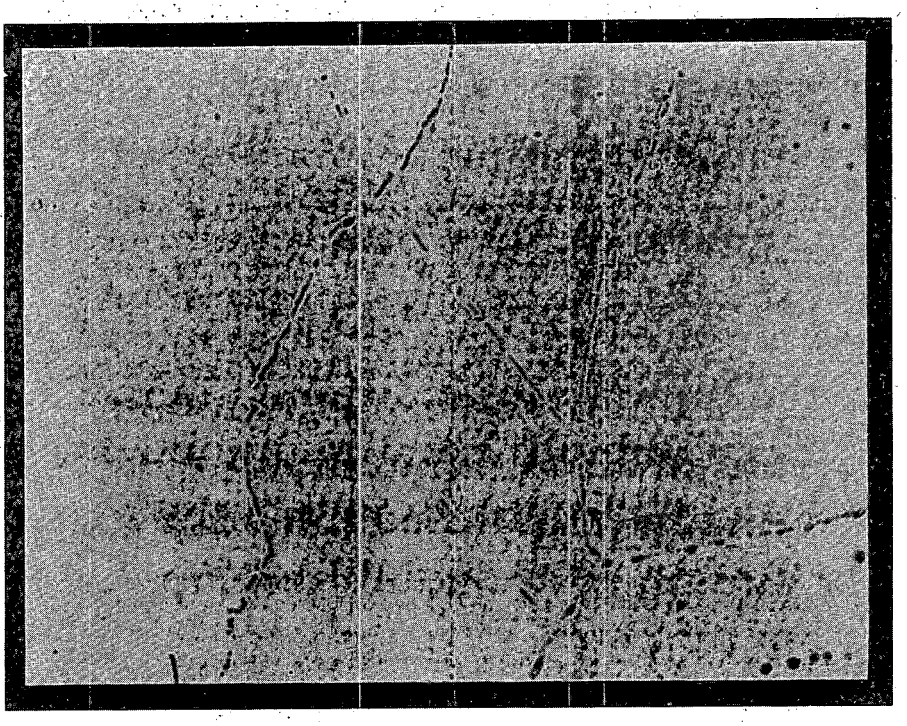

Test 10–2, $\Delta\dot{\epsilon}_t$ = 2.07%, $\dot{\epsilon}_t = 4.10 \times 10^{-5}$ sec^{-1} (Neg. 10139)

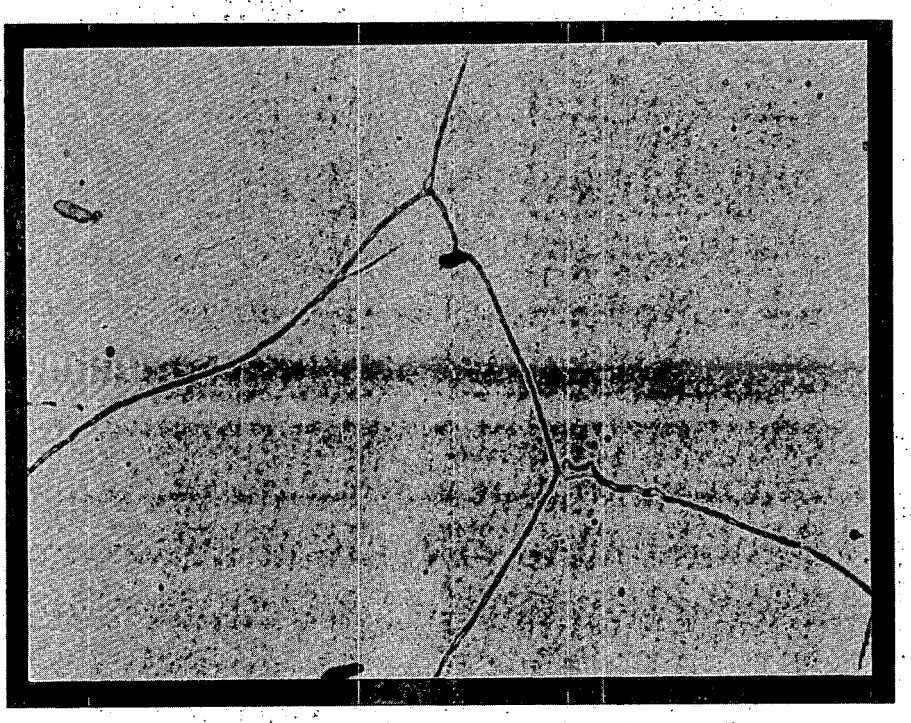

Test 7–1, $\Delta\dot{\epsilon}_t$ = 2.08%, $\dot{\epsilon}_t = 4.2 \times 10^{-3}$ sec^{-1} (Neg. 10138)

Fig. 6.28 – Photomicrographs taken near the crack initiation point showing the grain boundary phase in AISI 304 stainless steel tested at 816°C. ($22H_2SO_4$, $12H_2O_2$ [30%], $66H_2O$, electrolytic etchant; 1000X)

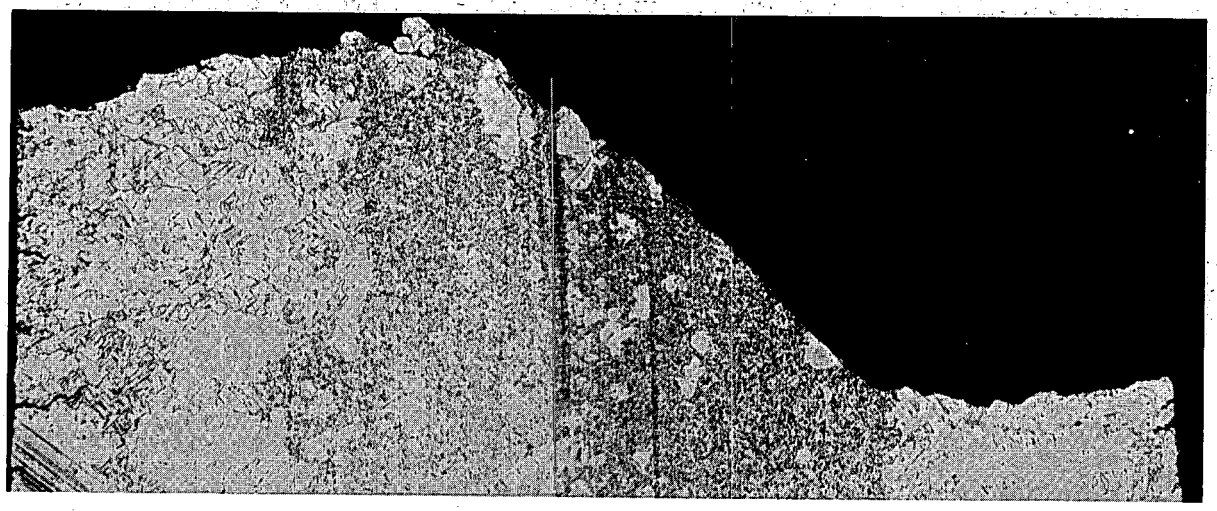

Neg. 10067 Test 3–7, $\Delta\dot{\epsilon}_t = 2.17\%$, $\dot{\epsilon}_t = 4.3 \times 10^{-5}\ sec^{-1}$ Neg. 10068

Neg. 10124 Test 3–8, $\Delta\dot{\epsilon}_t = 2.18\%$, $\dot{\epsilon}_t = 4.4 \times 10^{-4}\ sec^{-1}$ Neg. 10123

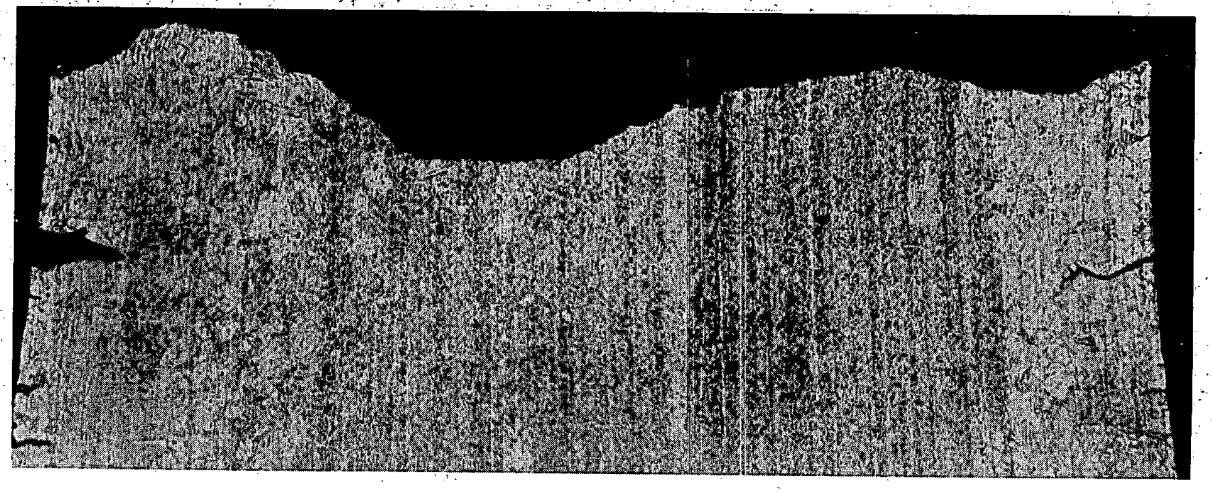

Neg. 10122 Test 3–4, $\Delta\dot{\epsilon}_t = 2.19\%$, $\dot{\epsilon}_t = 4.4 \times 10^{-3}\ sec^{-1}$ Neg. 10121

Fig. 6.29 — Composite photomicrograph of longitudinal cross section of AISI 348 stainless steel tested at 650°C. ($22H_2SO_4, 12H_2O_2$ [30%], $66H_2O$, electrolytic etchant; ~25X)

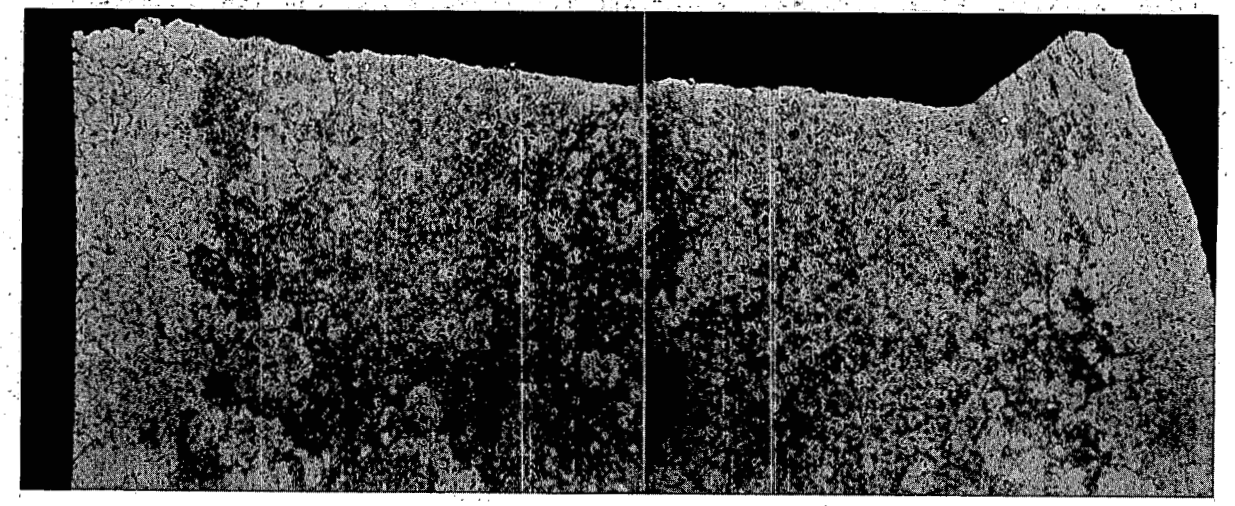

Neg. 10076 Test 5–12, $\Delta\dot{\epsilon}_t = 0.61\%$, $\dot{\epsilon}_t = 4.9 \times 10^{-5}\ sec^{-1}$ Neg. 10075

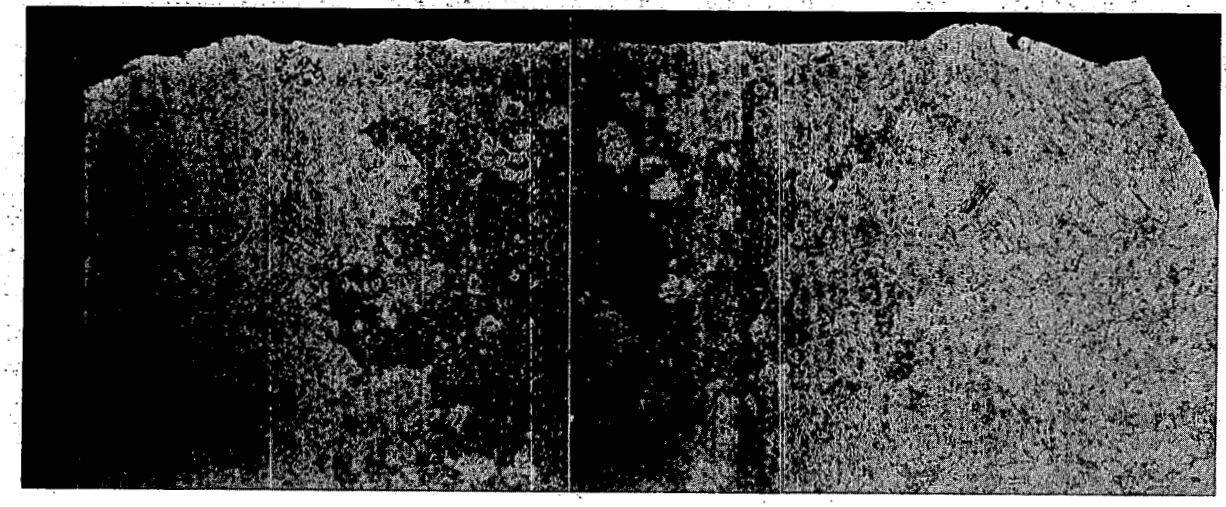

Neg. 10074 Test 3–11, $\Delta\dot{\epsilon}_t = 0.62\%$, $\dot{\epsilon}_t = 5.0 \times 10^{-4}\ sec^{-1}$ Neg. 10073

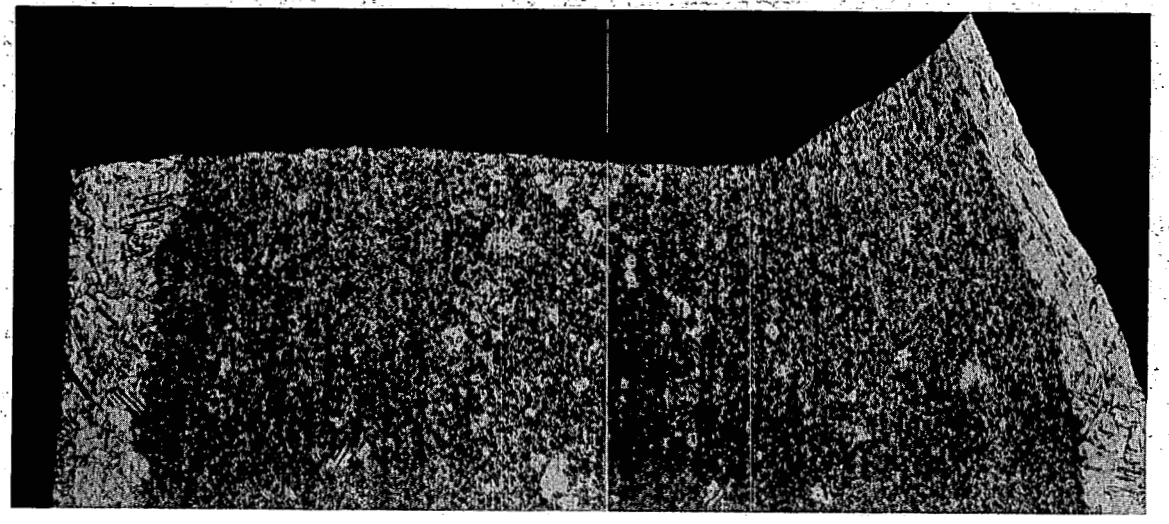

Neg. 10072 Test 5–3, $\Delta\dot{\epsilon}_t = 0.62\%$, $\dot{\epsilon}_t = 5.0 \times 10^{-3}\ sec^{-1}$ Neg. 10071

Fig. 6.30 — Composite photomicrograph of longitudinal cross section of AISI 348 stainless steel tested at 650°C. ($22H_2SO_4$, $12H_2O_2$ [30%], $66H_2O$, electrolytic etchant; ~25X)

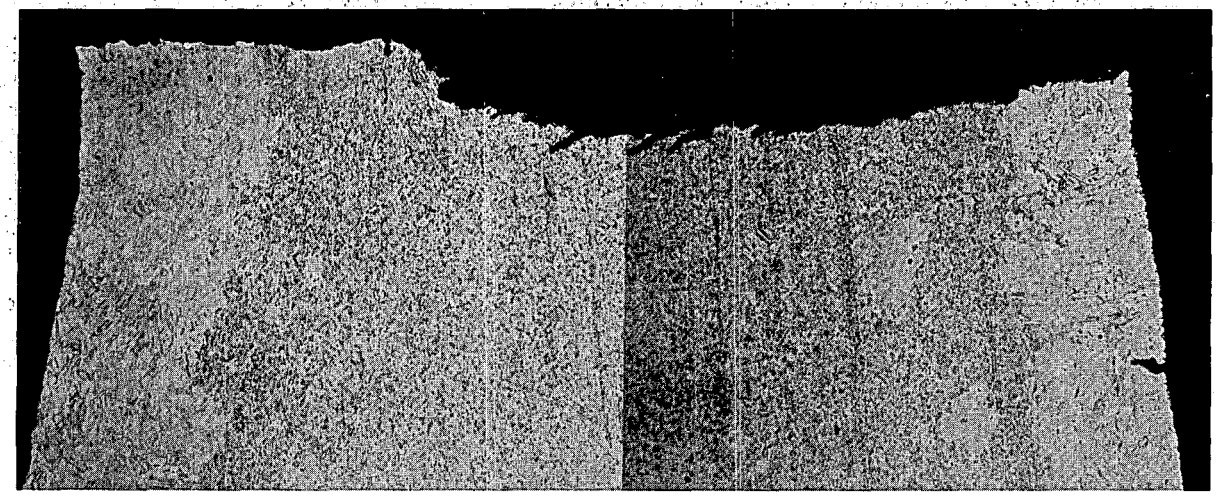

Neg. 10081 Test 6–10, $\Delta\dot{\epsilon}_t = 0.56\%$, $\dot{\epsilon}_t = 4.6 \times 10^{-5}\ sec^{-1}$ Neg. 10082

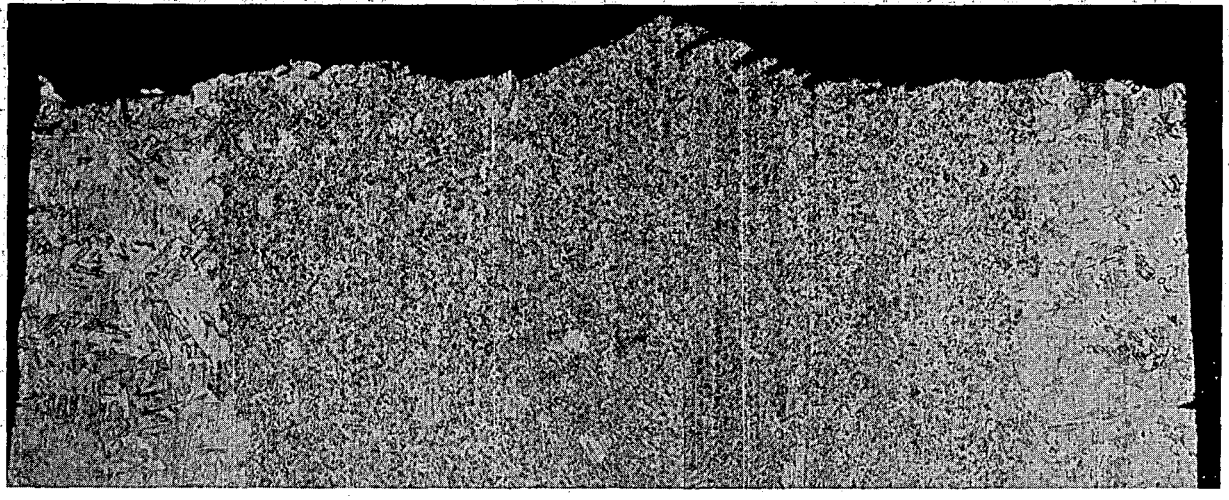

Neg. 10080 Test 6–8, $\Delta\dot{\epsilon}_t = 0.58\%$, $\dot{\epsilon}_t = 4.6 \times 10^{-4}\ sec^{-1}$ Neg. 10079

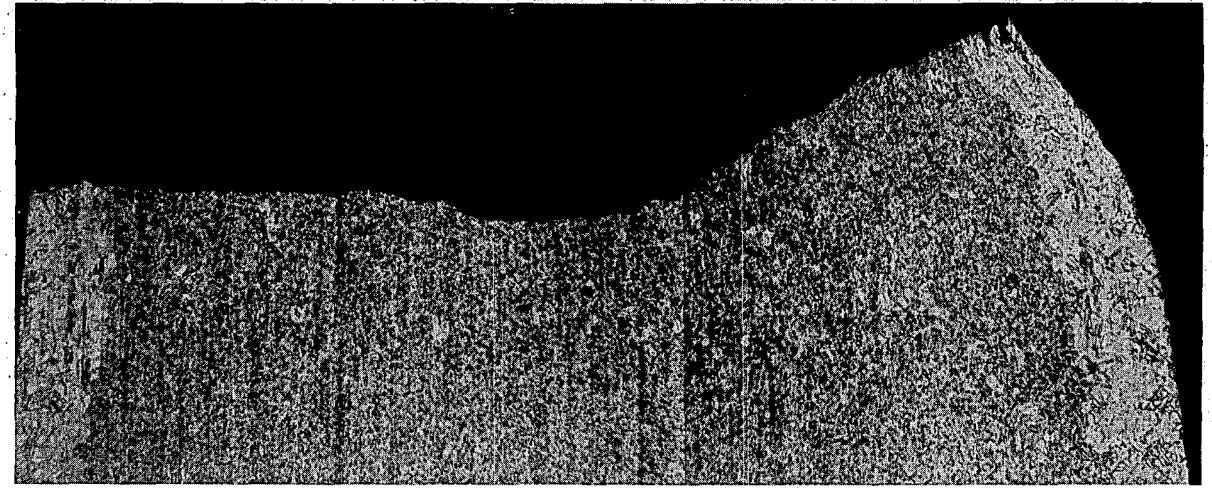

Neg. 10078 Test 6–2, $\Delta\dot{\epsilon}_t = 0.57\%$, $\dot{\epsilon}_t = 4.5 \times 10^{-3}\ sec^{-1}$ Neg. 10077

Fig. 6.31 — Composite photomicrograph of longitudinal cross section of AISI 348 stainless steel tested at 816°C. ($22H_2SO_4$, $12H_2O_2$ [30%], $66H_2O$, electrolytic etchant; ~25X)

TABLE 6.6

FRACTURE MODE CHARACTERIZATION OF AISI 304 AND 348 STAINLESS STEEL LOW-CYCLE FATIGUE SPECIMENS

Specimens	Test Temperature, °C	Test No.	Axial Strain Range ($\Delta\dot{\epsilon}_t$), %	Axial Strain Rate ($\dot{\epsilon}_t$), sec^{-1}	Cycles to 5 % Reduction in Load (N_5)	Mode Crack Initiation	Intergranular Crack Length from Point of Initiation, mm	Mode of Crack Propagation to the Shear Point	Specific Observations
304 SS	650	10-12	2.12	4.2×10^{-5}	197	Intergranular	0.3	Inter- + transgranular	Continuous unidentified phase observed in grain boundaries; etch pits in highly strained regions.
	650	10-11	2.15	4.3×10^{-4}	287	Intergranular	0.1	Primarily transgranular	
	650	10-9	2.11	4.2×10^{-3}	524	Transgranular	–	Primarily transgranular	
	650	120	0.58	4.6×10^{-5}	1,533	Intergranular	0.6	Inter- + transgranular	Continuous unidentified phase observed in grain boundaries; etch pits in highly strained region.
	650	296	0.60	4.8×10^{-4}	3,009	Intergranular	0.2	Primarily transgranular	
	650	294	0.62	4.9×10^{-3}	7,176	Transgranular	–	Primarily transgranular	
	816	10-2	2.07	4.1×10^{-5}	80	Intergranular	4.0	Primarily intergranular	Intermittent unidentified phase observed in grain boundaries; subgrains in highly strained regions.
	816	7-3	2.07	4.1×10^{-4}	117	Intergranular	1.2	Primarily intergranular	Continuous unidentified phase observed in grain boundaries; a few etch pits and subgrains in highly strained regions.
	816	7-1	2.08	4.2×10^{-3}	226	Intergranular	1.0	Primarily intergranular	Continuous unidentified phase observed in grain boundaries; few etch pits in highly strained regions.

TABLE 6.6 (Cont.)

FRACTURE MODE CHARACTERIZATION OF AISI 304 AND 348 STAINLESS STEEL LOW-CYCLE FATIGUE SPECIMENS

Specimens	Test Temperature, °C	Test No.	Axial Strain Range ($\Delta\dot{\epsilon}_t$), %	Axial Strain Rate ($\dot{\epsilon}_t$), sec^{-1}	Cycles to 5% Reduction in Load (N_5)	Mode Crack Initiation	Intergranular Crack Length from Point of Initiation, mm	Mode of Crack Propagation to the Shear Point	Specific Observations
	816	10-3	0.53	4.2×10^{-5}	591	Intergranular	0.7	Primarily intergranular	Intermittent unidentified phase observed in grain boundaries; no etch pits in highly strained regions.
	816	7-7	0.54	4.3×10^{-4}	1,055	Intergranular	0.8	Primarily intergranular	Continuous unidentified phase observed in grain boundaries; etch pits in highly strained regions.
	816	7-9	0.56	4.5×10^{-3}	2,346	Intergranular	0.8	Primarily intergranular	Continuous unidentified phase in grain boundaries; subgrains in highly strained regions.
348 SS	650	3-7	2.17	4.3×10^{-5}	193	Intergranular	0.2	Transgranular	Large amounts of secondary cracking; grain boundaries were relatively clean compared to 304 SS.
	650	3-8	2.18	4.4×10^{-4}	320	Intergranular	0.1	Transgranular	
	650	3-4	2.19	4.4×10^{-3}	585	Intergranular	0.1	Transgranular	
	650	5-12	0.61	4.9×10^{-5}	5,464	Intergranular	0.4	Transgranular	Limited secondary cracking; crack propagation was very regular, flat, and perpendicular to specimenn axis.
	650	3-11	0.62	5.0×10^{-4}	10,948	Intergranular	0.2	Transgranular	
	650	5-3	0.62	5.0×10^{-3}	15,010	Intergranular	0.1	Transgranular	
	816	5-7	2.06	4.1×10^{-5}	122	Intergranular	<0.1	Transgranular	Numerous secondary cracks.
	816	5-5	2.11	4.2×10^{-4}	158	Intergranular	<0.1	Transgranular	
	816	5-1	2.11	4.2×10^{-3}	266	Intergranular	<0.1	Transgranular	
	816	6-10	0.56	4.6×10^{-5}	1,613	Intergranular	<0.1	Transgranular	Crack propagation was very regular, flat, and almost perpendicular to specimen axis; cracks developed at ~60 degree angle to primary fracture surface in the direction of propagation.
	816	6-8	0.58	4.6×10^{-4}	2,718	Intergranular	<0.1	Transgranular	
	816	6-2	0.57	4.5×10^{-3}	4,656	Intergranular	<0.1	Transgranular	Crack propagation was very regular, flat, and perpendicular to specimen axis.

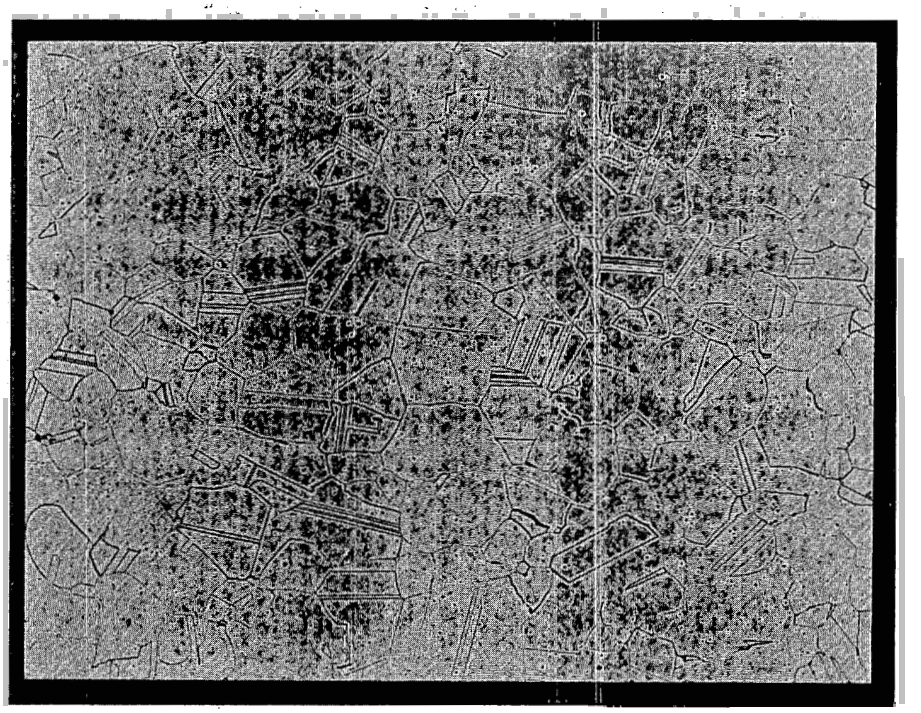

Fig. 6.32 — Photomicrograph showing pre-test structure of AISI 316 stainless steel (longitudinal cross section) used in low-cycle fatigue testing. (Neg. 10083; $22H_2SO_4$, $12H_2O_2$ [30%], $66H_2O$, electrolytic etchant; 100X)

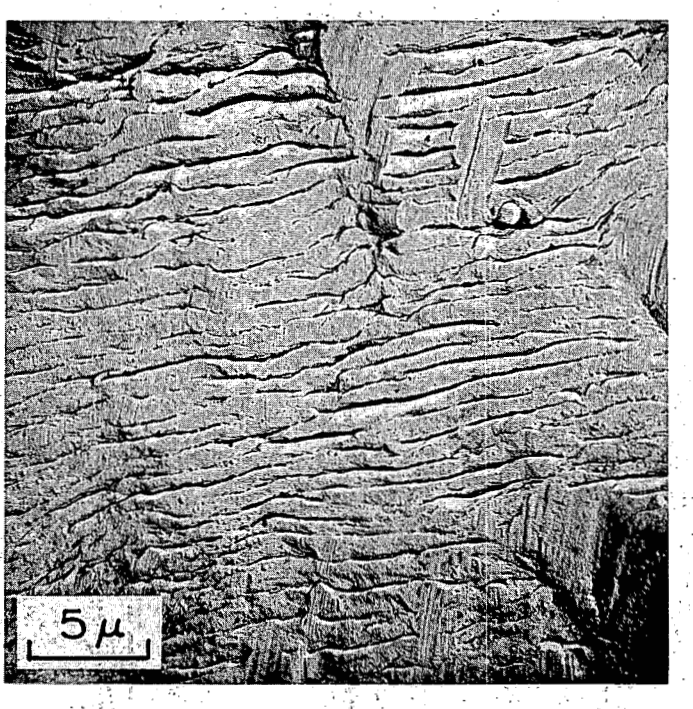

Fig. 6.33 — Electron fractograph showing striations on the fractured surface of AISI 304 stainless steel tested at 0.51% strain range, $4.5 \times 10^{-3} sec^{-1}$ strain rate, and 430°C. Note rub-marks in the top center portion of the fractograph (two-stage acetate-carbon replica). Test No. 347U (Neg. 1197B)

Low-cycle fatigue data were generated for AISI 348, 304, and 316 stainless steel to determine effects of strain range (0.3 to 2.2 percent), temperature, (430°, 650°, and 816°C), and strain rate, (4×10^{-3}, 4×10^{-4}, and 4×10^{-5} sec^{-1}).

In general, the 348 SS exhibited slightly better strain fatigue resistance for a given total axial or plastic strain level than 304 or 316 SS; this effect was observed for all three temperatures evaluated. The fatigue resistance of 316 SS for 650°C, however, is less than either the 304 or 348 SS. The 348, 304, and 316 SS exhibited cyclic strain-hardening characteristics for the various test conditions evaluated, except for the 316 SS tested at 430°C. The 316 SS exhibited cyclic strain hardening followed by cyclic strain softening over the entire strain range evaluated.

Results for 348 and 316 SS tested at 430°C are in fair agreement with the Coffin-Manson relationship that correlates low-cycle fatigue life at temperatures below the creep range. Fair agreement was obtained using the Manson-Halford approach for predicting the fatigue life of materials tested in the creep range. In general data tended to be more conservative than the average prediction had indicated.

A hundredfold decrease in strain rate caused a severalfold decrease in the fatigue resistance of 304 and 348 SS tested at 650°C and 816°C. Similar results were obtained for 316 SS tested at 650°C. At a test temperature of 816°C, however, only slight differences in the fatigue resistance of 316 SS were observed at strain ranges less than 1.0 percent for a change in strain rate from 4×10^{-4} sec^{-1} to 4×10^{-5} sec^{-1}. This improvement in the fatigue characteristics of 316 SS at the lowest strain rate is presumably due to a metallurgical reaction.

The shape of the curves shown in plots of total axial or plastic strain versus fatigue life, N_5, for the three materials evaluated does not seem to change as the strain rate is decreased several hundredfold but the curve is shifted to positions of lower life for given strain values.

A comparison of the ratio of N_5/N_f for the overall data showed that this ratio is generally decreased from a range of approximately 0.99 to 0.90 representing the 650°C data, to a range of approximately 0.7 to 0.85 for the 816°C data.

An attempt was made to characterize the N_5 failure criterion from the standpoint of crack length. Preliminary results of a fractographic analysis for samples tested at 650°C indicate that the crack is approximately 1.7 mm long at the N_5 point.

Results of a metallographic and fractographic analysis of 348 and 304 SS specimens tested at 650°C and 816°C and strain rates of 4×10^{-3}, 4×10^{-4}, and 4×10^{-5} sec^{-1}, showed that the mode of crack initiation was primarily intergranular for all conditions tested, except for the highest strain rate at 650°C. Under these conditions the 304 SS exhibited a transgranular type of crack initiation at both the highest and lowest strain range evaluated.

6.7 PLANS AND RECOMMENDATIONS

The effect of strain rate on fatigue characteristics of AISI 348, 304, and 316 stainless steels will be further evaluated. This continuing work will duplicate several test conditions for which only a few data points are presently available. Overall data will be statistically analyzed when these tests are completed. Several tests will also be conducted to determine the strain-rate sensitivity at 430°C of the austenitic stainless steels presently being evaluated.

Testing will be initiated to determine the effect of hold times at peak strain for AISI 348, 304, and 316 stainless steels. These data will be obtained at temperatures of 430°, 650°, and 816°C.

The various aspects of biaxial fatigue testing are being investigated. Several techniques are being reviewed for conducting biaxial fatigue tests at NMPO.

Metallographic and fractographic analyses of fatigue specimens will continue. Special emphasis is being placed on fracture analysis, although future work will include an investigation of morphology changes in the various materials being evaluated.